NASA MEMO 5-1-59H

NASA

MEMORANDUM

FLOW CHARACTERISTICS ABOUT TWO THIN WINGS OF LOW ASPECT RATIO DETERMINED FROM SURFACE PRESSURE MEASUREMENTS OBTAINED IN FLIGHT AT MACH NUMBERS FROM 0.73 TO 1.90

By Norman V. Taillon

High-Speed Flight Station
Edwards, Calif.

NATIONAL AERONAUTICS AND SPACE ADMINISTRATION
WASHINGTON
May 1959
Declassified July 11, 1961

NATIONAL AERONAUTICS AND SPACE ADMINISTRATION

MEMORANDUM 5-1-59H

FLOW CHARACTERISTICS ABOUT TWO THIN WINGS OF LOW ASPECT RATIO DETERMINED FROM SURFACE PRESSURE MEASUREMENTS OBTAINED IN FLIGHT AT MACH NUMBERS FROM 0.73 TO 1.90

By Norman V. Taillon

SUMMARY

Surface pressure measurements were obtained at three chordwise stations on the wings of the X-3 and X-1E airplanes at Mach numbers from 0.73 to 1.13 for the X-3, and from 0.82 to 1.90 for the X-1E.

Leading-edge separation is present on the X-3 wing at a Mach number of about 0.73 and an angle of attack of about 6°. However, when the Mach number is increased to 0.88, the trailing-edge separation dominates the pressure distribution and no leading-edge separation is visible although it is anticipated at the higher angles of attack shown. Conversely, the X-1E wing shows no indication of leading-edge separation within the scope of this investigation, but an overexpansion immediately behind the leading edge is present at a Mach number of approximately 0.82.

Two separate normal shocks are present on the X-3 wing at a Mach number of about 0.88 and at a low angle of attack as an effect of wing geometry. These shocks merge to form a single shock when the angle of attack is increased to about 6°.

At supersonic speeds the upper-surface expansion on the X-1E wing is limited by the approach of the pressure coefficients to the pressure coefficient for a vacuum.

INTRODUCTION

Pressure surveys were conducted over the upper and lower surfaces of the X-3 and X-1E wings during flight tests performed at the NASA High-Speed Flight Station at Edwards, Calif. These data are employed in this paper to form the basis for analysis of the flow about the wings of the two airplanes as affected by Mach number and angle of attack, and analysis of the effect of the flow behavior on the section normal-force and moment coefficients. Measurements were obtained at root, midsemispan, and tip stations at Mach numbers from about 0.73 to 1.13 for the X-3, and from about 0.82 to 1.90 for the X-1E.

Wing pressure measurements and load distributions were previously reported separately for the two airplanes. Preliminary surface pressure distributions at a midsemispan station on the X-3 wing were reported in reference 1, resultant load distributions from five chordwise stations and a Mach number-angle-of-attack boundary for leading-edge separation in reference 2, and the effect of deflecting the leading-edge flap on the wing loads in reference 3. Reference 4 is representative of wind-tunnel investigations treating the subject of leading-edge separation. Chordwise and spanwise loadings of the X-1E wing were compared with theory at subsonic, sonic, and supersonic speeds in reference 5.

All pressure distributions obtained in the investigation from which the data herein were selected are available in tabular form from the NASA.

SYMBOLS

c local wing chord, ft

$c_{m_{c/4}}$ section pitching-moment coefficient about the local quarter chord, $\int_0^1 \Delta C_p \left(0.25 - \frac{x}{c}\right) d\frac{x}{c}$

c_n section normal-force coefficient, $\int_0^1 \Delta C_p \, d\frac{x}{c}$

C_p pressure coefficient, $\frac{p - p_0}{q}$

ΔC_p differential pressure coefficient, $\frac{p_l - p_u}{q}$

$C_{p_{cr}}$ critical pressure coefficient (local Mach number equals 1.0)

$C_{p_{ult}}$ ultimate pressure coefficient, $-\frac{1}{0.7M^2}$

M free-stream Mach number

p local static pressure, lb/sq ft

p_l local static pressure on lower wing surface, lb/sq ft

p_0 free-stream static pressure, lb/sq ft

p_u local static pressure on upper wing surface, lb/sq ft

q free-stream dynamic pressure, lb/sq ft

x chordwise distance rearward of leading edge, ft

α wing angle of attack, deg

DESCRIPTION OF AIRPLANES AND WINGS

Photographs of the X-3 and X-1E airplanes are shown in figures 1 and 2, respectively. Three-view drawings presenting the overall dimensions are shown in figures 3 and 4, and drawings of the wings, showing the locations of the orifice rows, in figures 5 and 6. The geometric characteristics of the wings of the two airplanes are given in table I. Wing section ordinates are shown in tables II and III.

The X-3 wing is a 4.5-percent-thick airfoil with a hexagonal cross section modified at the 30- and 70-percent-chord vertices by 188-inch radii. Small radii are also used to round off the leading and trailing edges as shown in table II. The wing has an aspect ratio of 3.09, a taper ratio of 0.39, and zero incidence, dihedral, and twist.

The X-1E wing employs the NACA 64A-004 airfoil section, with the portion of the wing rearward of the 70-percent-chord line modified so that the trailing edge has a thickness equal to 0.0036c. The wing has an aspect ratio of 4.0, a taper ratio of 0.50, and incidence of 2°. Dihedral and twist are zero.

Orifice rows are located at 30.1, 62.4, and 91.1 percent of the 11.344-foot left wing of the X-3, and at 23.4, 57.0, and 92.9 percent

of the 11.395-foot left wing of the X-1E. Chordwise locations of the orifices are presented in tables IV and V.

INSTRUMENTATION AND ACCURACY

Standard NASA film-recording instruments were employed to record wing static pressures, Mach number, and angle of attack. Individual pressure measurements were obtained from static-pressure orifices installed flush with the wing skin and connected by tubing to NASA recording mechanical manometers. All recording instruments were synchronized by a common timer. Lag was negligible for the data presented herein.

Probable accuracies determined for the data of this paper are:

M	±0.01
C_p	±0.02
c_n	±0.03
$c_{m_{c/4}}$	±0.01
α, deg	±1

TESTS

The data for this investigation were obtained during wind-up turns at Mach numbers from about 0.72 to about 1.90 at altitudes between 30,000 and 70,000 feet. Rolling and pitching velocities and accelerations were monitored as a check to insure that near-steady-state conditions prevailed. All data were obtained with the airplanes in the clean configuration.

DISCUSSION

X-3 Pressure Distribution

Surface pressure measurements from the X-3 wing are shown in figure 7. These data provide the basic information from which the flow characteristics are inferred. At a Mach number of 0.73 (fig. 7(a)) and angle of attack of about 3°, the X-3 pressure distribution shows a moderate leading-edge negative-pressure peak. This peak continues to expand as angle of attack increases; however, at $\alpha = 6.2°$ the

termination of expansion at the midsemispan station suggests the presence of leading-edge separation. Reference 6 points out that a region of essentially constant pressure immediately behind the leading edge is indicative of leading-edge separation associated with a stall of the thin-wing type, and reference 7, which presents tuft studies of an X-3 model, shows that leading-edge separation may be expected at an angle of attack of about 4° at Mach numbers below 0.80. A further increase in angle of attack to 9.8° extends the separation to the other stations. When the Mach number is increased to about 0.88, leading-edge separation would be expected to occur at an angle of attack of about 9° at the tip station (ref. 2). However, at angles of attack of 8.6° and 10° (fig. 7(b)), trailing-edge separation (denoted by the failure of the pressures to fully recover at the trailing edge) dominates the pressure distribution, and no clear evidence of leading-edge separation is visible.

The shock system that can be inferred from figure 7(b) is of particular interest. On the upper surface at $\alpha = 2.4^\circ$ the flow expands over the front vertex (30-percent chord) attains a partial pressure recovery through a shock behind the vertex, then undergoes a second expansion over the rear vertex (70-percent chord) also followed by a shock and pressure recovery. A shock is also present at the lower-surface rear vertex. At an angle of attack of about 6° the upper-surface shocks consolidate to form a single strong shock at about 50-percent chord, while the lower-surface shocks retain about the same structure as shown for the lower angle of attack. The strong upper-surface shock, identified by the abrupt pressure recovery, is situated at about 60-percent chord at an angle of attack of 7.1°. As the angle of attack increases to 8.6°, the shock is, in general, made indistinct by the previously mentioned flow separation. On the lower surface the flow expansion and associated shock has moved to the rear of the vertex, except at the root station which is subcritical. Other than more extensive separation at the tip, no appreciable change is noted with the increase of α to 10°.

At a Mach number of 0.99 (fig. 7(c)) the pressures on the upper surface of the wing at $\alpha = 3.0^\circ$ are marked by an area immediately rearward of the leading edge where the expanded flow is terminated through a sharp pressure recovery. This is followed by an accelerating supersonic flow over the remainder of the surface. The lower surface shows a more linear acceleration of the flow from positive pressure at the leading edge to a negative-pressure supersonic expansion over most of the airfoil surface. At the higher angles of attack the pressure distributions approach the rectangular shape associated with supersonic flow. This Mach number is well above that for which leading-edge separation may be expected.

Little change in the pressure distributions, and therefore in the flow characteristics, is noted for the X-3 as Mach number is increased to about 1.13 (fig. 7(d)). Again, at an angle of attack of 3.0°, a pressure recovery and subsequent expansion is evident behind a small leading-edge peak. Increases in angle of attack to a maximum of 16.9° result in a relevant expansion of the pressure distributions without the deleterious effects experienced in the transonic range. Fuselage interference results in somewhat lower negative-pressure coefficients on the upper-surface root station than at the other stations.

X-1E Pressure Distribution

The X-1E wing at a Mach number of 0.82 (fig. 8(a)) shows evidence of overexpansion on the forward part of the upper surface, probably as an effect of the rather sharp leading edge. This results in the formation of a modest negative-pressure peak, followed in turn by a partial pressure recovery and a secondary expansion. The overexpansion is particularly evident at the root station and is present at all angles of attack for Mach numbers of 0.88 and 0.90 (figs. 8(b) and 8(c)) as well as for the lower speed previously mentioned. No indication of leading-edge separation is noted for the X-1E wing within the scope of this investigation, although reference 4 suggests that leading-edge separation might be expected at about the maximum angle of attack recorded at a Mach number of 0.82 (fig. 8(a)).

The shock position on the X-1E wing at low lift may be observed from the pressure distributions for an angle of attack of about 4° in figures 8(a) to 8(c). The shock is at about 30-percent chord at $M \approx 0.82$, moving rearward to about 55-percent chord at $M \approx 0.88$, and to about 65-percent chord at $M \approx 0.90$. Flow separation obscures the shock position at higher angles of attack and is responsible for the failure of the surface pressures to recover at the trailing edge.

At a Mach number of about 1.25 (fig. 8(d)) the shock is located at the trailing edge and supersonic flow exists over both surfaces of the wing. It will be noted that the upper-surface expansion is limited by the approach of the pressure coefficients to those for a vacuum, thus tending to promote an equal distribution of pressure along the wing chord. (The ultimate pressure coefficient $C_{p_{ult}}$ indicated on the root stations in the figures also applies to the midsemispan and tip stations, but is omitted from the latter two in the interest of clarity.) The upper-surface pressures become more highly restricted as Mach number increases, as shown in figures 8(e) and 8(f). At $M = 1.77$ and $\alpha = 6.3°$ (fig. 8(e)) a positive pressure is evident on the upper-surface leading edge at the midsemispan and tip stations. This pressure diminishes with increasing angle of attack, but does not become negative

at all stations until an angle of attack of about 11° has been attained. At $M \approx 1.90$ (fig. 8(f)) the upper-surface leading-edge pressure does not become negative at all stations below an angle of attack of about 13.5°. The foregoing is attributed to the reduction in aerodynamic angle of attack caused by a reduction in upwash associated with symmetrical airfoils at supercritical Mach numbers. The reduced pressure coefficient of the lower surface at about 75-percent chord of the midsemispan station, visible in figures 8(d) to 8(f), is believed to be caused by disturbed flow about the flap-hinge brackets.

Effect of Flow Behavior on the Section Normal-Force Coefficients

Section normal-force curves are presented in figures 9 and 10 for the X-3 and X-1E, respectively. At subsonic speeds ($M = 0.73$ to 0.90) the root and midsemispan stations of the two wings attain maximum section normal-force coefficients of about 0.7 to 0.8, with the tip stations reaching a somewhat lower level. The maximum section normal-force coefficients are limited by upper-surface-flow separation at subsonic speeds of both airplanes as discussed previously and illustrated in figures 7 and 8. For the X-3 the separation starts at the leading edge at $M \approx 0.73$, while at $M \approx 0.88$ the separation is shock-induced and occurs first over the rear portion of the wing. For the X-1E the separation is shock-induced at all subsonic speeds, although leading-edge separation could be expected at lower Mach numbers than reported in this paper.

At Mach numbers of 0.99 and greater the local flow over both wings is mostly supersonic. A reduction in the slope of the curves will be noted as Mach number increases; however, a higher overall c_n is recorded for both airplanes. Although there is evidence of trailing-edge separation on the X-3 wing, the effect on the lift is minor except at the higher angles of attack.

Effect of Flow Behavior on the Section Pitching-Moment Coefficients

The variation of section pitching-moment coefficient with angle of attack, figures 11 and 12, respectively, is generally unstable at subsonic speeds and low-to-moderate angles of attack for both airplanes. This is the result of high lift concentrated at the leading edge of the X-3 wing at a Mach number of 0.73, and of normal shocks which further reduce the lift over the rear portion of both airfoils at Mach numbers between 0.80 and 1.00. At the higher angles of attack greater lift is

present on the rear part of the airfoils as an effect of trailing-edge-flow separation, and the more uniform chordwise pressure distribution promotes the stable trend.

At supersonic speeds the wings become stable as the shock moves rearward and the leading-edge-suction peak diminishes. An exception to the stable trend may be noted for the X-3 at a Mach number of about 1.13 and high angle of attack (fig. 11). Reference to figure 7(d) shows that trailing-edge separation at the midsemispan station progresses forward from near the trailing edge at $\alpha = 12.3^{\circ}$ to about the midchord position at $\alpha = 16.9^{\circ}$. The root station also shows evidence of trailing-edge separation at the latter angle of attack. The section normal-force coefficients (fig. 9) indicate an incipient stall beginning at an angle of attack of about 16° at $M \approx 1.13$, which accounts for the previously mentioned unstable trend for the X-3.

CONCLUSIONS

Analysis of in-flight surface pressure measurements taken over the left wings of the X-3 and X-1E airplanes at Mach numbers ranging from 0.73 to 1.90 indicates that:

1. Leading-edge separation is present on the X-3 wing at a Mach number of about 0.73 and an angle of attack of about 6°; however, when the Mach number is increased to 0.88, trailing-edge separation dominates the pressure distribution and no leading-edge separation is visible although it is anticipated at the higher angles of attack.

2. The X-1E wing shows evidence of overexpansion at the lowest Mach number tested (0.82), but does not exhibit leading-edge separation within the scope of this investigation.

3. Two distinct normal shocks are attached to the vertices of the X-3 wing at a Mach number of approximately 0.88 and at a low angle of attack as an effect of wing geometry. These shocks merge to form a single shock located between the vertices when the angle of attack is increased to about 6°.

4. At supersonic Mach numbers the maximum pressure coefficients attainable on the upper surface of the two wings are restricted by their approach to the pressure coefficient for a vacuum.

High-Speed Flight Station,
National Aeronautics and Space Administration,
Edwards, Calif., February 12, 1959.

REFERENCES

1. Jordan, Gareth H., and Hutchins, C. Kenneth, Jr.: Preliminary Flight-Determined Pressure Distributions Over the Wing of the Douglas X-3 Research Airplane at Subsonic and Transonic Mach Numbers. NACA RM H55A10, 1955.

2. Keener, Earl R., and Jordan, Gareth H.: Wing Loads and Load Distributions Throughout the Lift Range of the Douglas X-3 Research Airplane at Transonic Speeds. NACA RM H56G13, 1956.

3. Keener, Earl R., McLeod, Norman J., and Taillon, Norman V.: Effect of Leading-Edge-Flap Deflection on the Wing Loads, Load Distributions, and Flap Hinge Moments of the Douglas X-3 Research Airplane at Transonic Speeds. NACA RM H58D29, 1958.

4. Lindsey, Walter F., and Landrum, Emma Jean: Compilation of Information on the Transonic Attachment of Flows at the Leading Edges of Airfoils. NACA TN 4204, 1958.

5. Malvestuto, Frank S., Cooney, Thomas V., and Keener, Earl R.: Flight Measurements and Calculations of Wing Loads and Load Distributions at Subsonic, Transonic, and Supersonic Speeds. NACA RM H57E01, 1957.

6. McCullough, George B., and Gault, Donald E.: Examples of Three Representative Types of Airfoil-Section Stall at Low Speed. NACA TN 2502, 1951.

7. Hamilton, William T., and Cleary, Joseph W.: Wind-Tunnel Tests of a 0.16-Scale Model of the X-3 Airplane at High Subsonic Speeds. Stability and Control Characteristics. NACA RM A50A03, 1950.

TABLE I.- WING GEOMETRY OF THE X-3 AND X-1E AIRPLANES

	X-3	X-1E
Airfoil section	Modified hexagon	NACA 64A-004 modified
Thickness ratio, percent local wing chord	4.5	4.0
Total area, sq ft	166.5	130.0
Span, ft	22.69	22.79
Mean aerodynamic chord, ft	7.84	5.92
Root chord, ft	10.58	7.62
Tip chord, ft	4.17	3.81
Taper ratio	0.39	0.50
Aspect ratio	3.09	4.0
Leading-edge sweep, deg	23.16	7.6
Trailing-edge sweep, deg	-8.12	-11.3
Incidence, deg	0	2
Dihedral, deg	0	0
Geometric twist, deg	0	0

TABLE II.- STATIONS AND ORDINATES OF THE MODIFIED HEXAGONAL AIRFOIL SECTION IN PERCENT OF LOCAL CHORD FOR THE X-3

Root		Midsemispan		Tip	
Station	Ordinate	Station	Ordinate	Station	Ordinate
0	±0.002	0	±0.003	0	±0.004
.028	±.032	.037	.042	.052	±.059
22.382	±1.709	19.948	±1.536	15.998	±1.255
25.990	±1.946	24.709	±1.848	22.643	±1.691
29.604	±2.115	29.477	±2.072	29.300	±2.002
33.219	±2.216	34.248	±2.206	35.960	±2.189
36.836	±2.250	39.023	±2.250	42.625	±2.251
63.602	±2.250	61.558	±2.250	58.264	±2.251
67.000	±2.218	66.043	±2.208	64.524	±2.192
70.397	±2.123	70.526	±2.082	70.782	±2.016
73.791	±1.964	75.005	±1.872	77.035	±1.725
77.183	±1.741	79.480	±1.579	83.282	±1.314
99.972	±.032	99.962	±.042	99.998	±.059
100.000	±.002	100.000	±.003	100.000	±.004

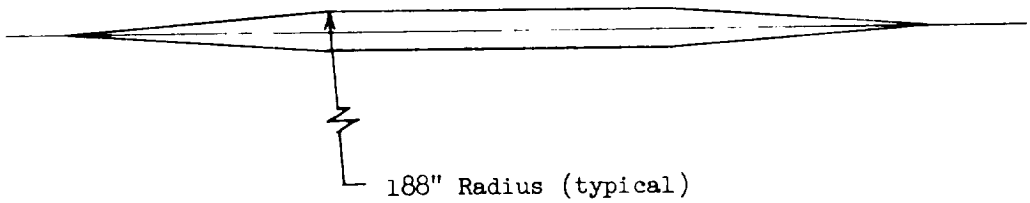

Profile of the X-3 wing

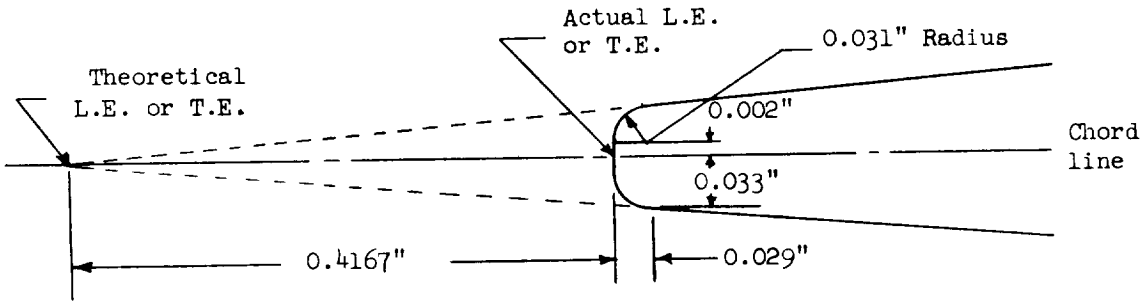

DIMENSIONS OF L.E. AND T.E.
(Same at all stations)

TABLE III.- STATIONS AND ORDINATES OF THE NACA 64A-004 AIRFOIL SECTION IN PERCENT OF LOCAL CHORD FOR THE X-1E

Station, percent local chord	Ordinate, percent local chord
0	0
.50	±.323
.75	±.390
1.25	±.493
2.50	±.678
5.0	±.932
7.5	±1.122
10.0	±1.278
15.0	±1.520
20.0	±1.702
25.0	±1.836
30.0	±1.929
35.0	±1.983
40.0	±1.999
45.0	±1.966
50.0	±1.889
55.0	±1.776
60.0	±1.634
65.0	±1.469
70.0	±1.282
75.0	±1.078
80.0	±.866
85.0	±.652
90.0	±.438
95.0	±.223
100.0	±.008

Note: The portion of the wing rearward of the 70-percent-chord line was modified so that the trailing edge had a thickness equal to 0.0036c.

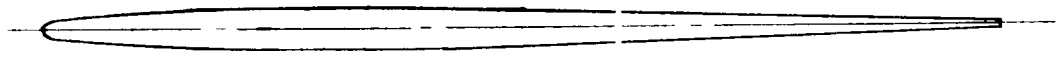

Profile of the X-1E wing

TABLE IV.- CHORDWISE LOCATION OF ORIFICES ON THE X-3 WING

[Percent local chord]

Upper Surface

Orifice	Station		
	Root	Midsemispan	Tip
2	2.1	2.5	5.2
4	5.0	4.8	7.4
6	7.8	7.3	14.4
8	9.3	10.1	24.6
10	15.3	17.8	29.0
12	20.0	20.2	37.9
14	25.0	24.4	47.3
16	29.5	29.5	61.9
18	37.4	37.9	68.2
20	47.6	47.4	75.6
22	55.5	55.0	79.9
24	62.0	64.6	84.5
26	69.0	68.7	90.0
28	74.2	74.1	92.4
30	80.0	80.0	97.4
32	85.4	85.0	
34	90.0	90.0	
36	92.5	92.5	
38	98.3	97.7	

Lower Surface

Orifice	Station		
	Root	Midsemispan	Tip
1	2.1	2.5	5.2
3	5.0	4.9	7.5
5	7.6	7.4	14.2
7	9.0	10.1	25.0
9	15.1	18.0	29.5
11	19.9	20.3	38.0
13	24.9	24.4	47.5
15	29.6	29.6	62.0
17	37.4	37.9	68.3
19	47.5	47.4	75.7
21	55.4	55.0	80.2
23	62.0	64.5	84.7
25	69.0	68.7	90.0
27	74.1	74.0	92.4
29	80.0	80.0	97.4
31	85.0	84.9	
33	90.0	90.0	
35	92.5	92.5	
37	98.1	97.7	

TABLE V.- CHORDWISE LOCATION OF ORIFICES ON THE X-1E WING

[Percent local chord]

Upper Surface

Orifice	Station		
	Root	Midsemispan	Tip
2	1.2	1.2	1.3
4	2.4	2.4	2.4
6	4.9	4.8	4.8
8	10.0	10.0	9.9
10	20.0	20.0	20.1
12	30.0	30.0	30.0
16	41.0	40.0	40.1
20	49.3	49.6	50.0
24	59.1	59.0	60.0
26	65.0	65.0	65.0
28	70.0	70.1	73.8
30	77.0	77.1	76.2
32	80.0	80.1	80.1
36	88.9	89.4	89.1
38	92.9	93.0	93.1
40	96.8	97.1	97.1

Lower Surface

Orifice	Station		
	Root	Midsemispan	Tip
1	0	0	0
3	1.2	1.3	1.3
5	2.4	2.6	2.6
7	5.0	5.2	5.1
9	10.0	10.1	10.1
11	20.0	20.1	20.1
13	30.0	30.1	30.2
17	41.0	40.0	40.0
21	49.3	49.5	50.0
25	59.1	59.4	60.0
29	69.9	70.0	65.1
31	77.0	77.9	73.7
33	80.0	80.1	76.3
37	88.9	89.4	80.3
39	92.2	93.2	89.2
41	96.9	97.0	97.4

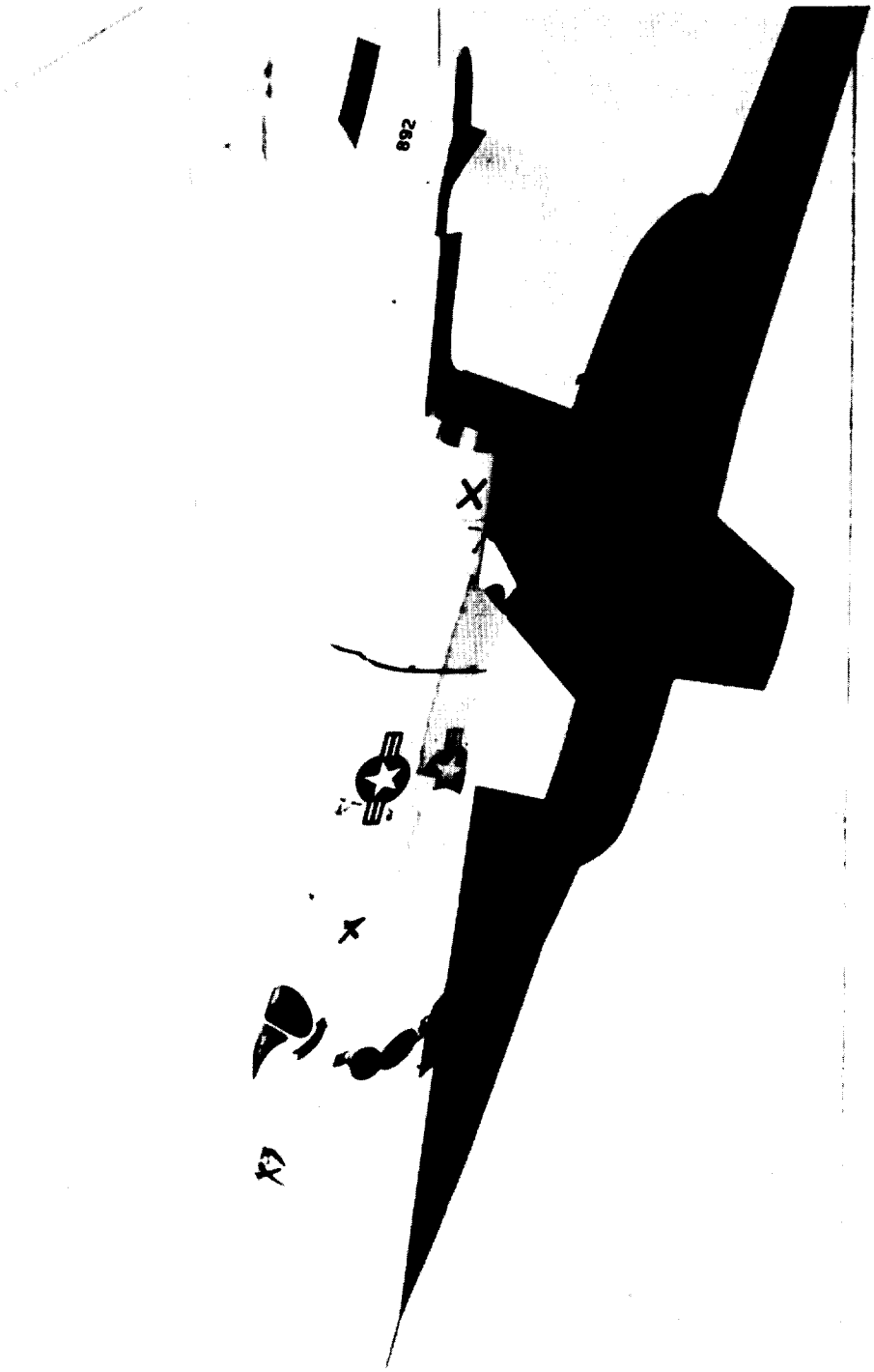

Figure 1.- Photograph of the X-3 airplane. E-1996

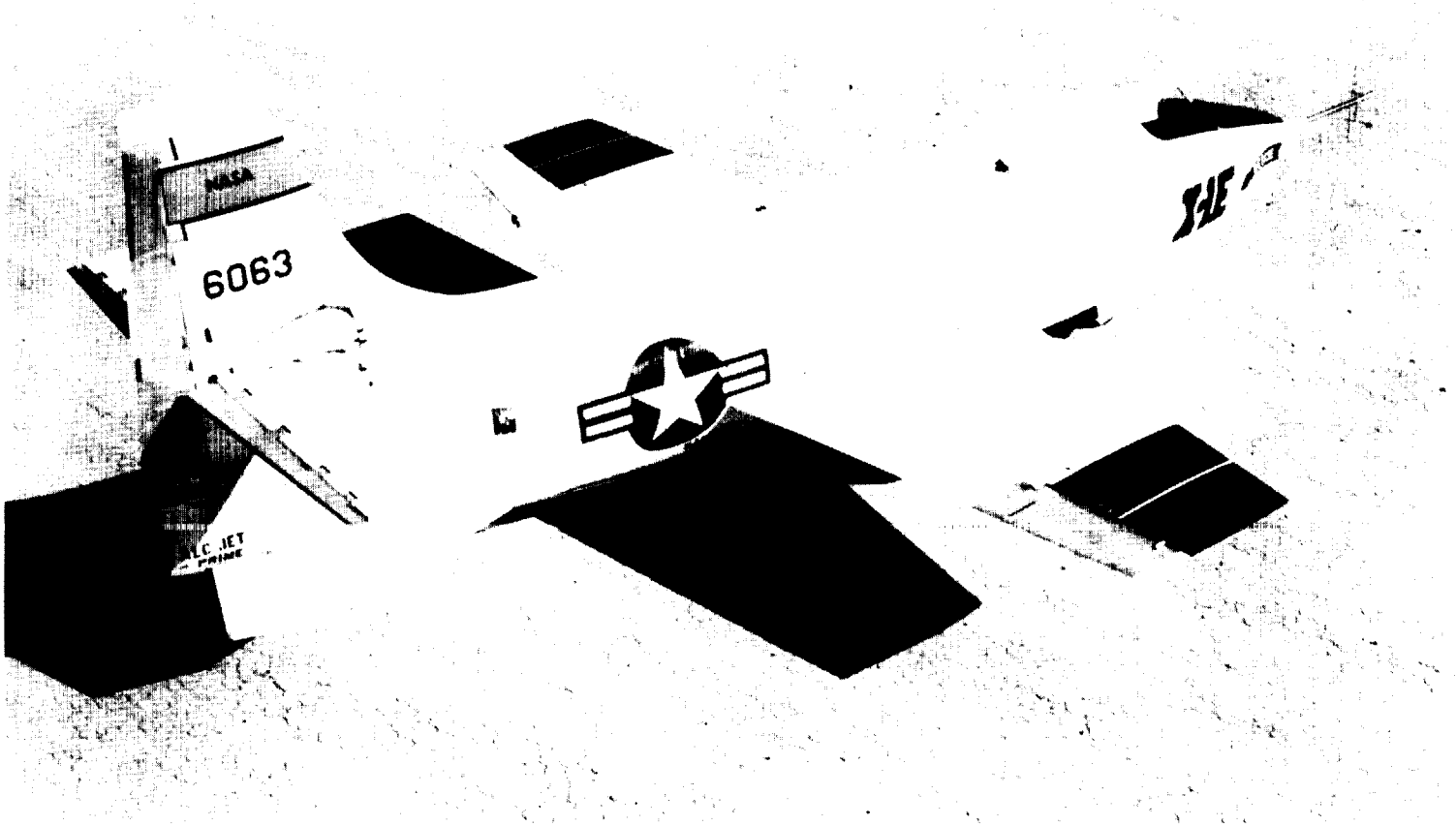

Figure 2.- Photograph of the X-1E airplane. E-4363

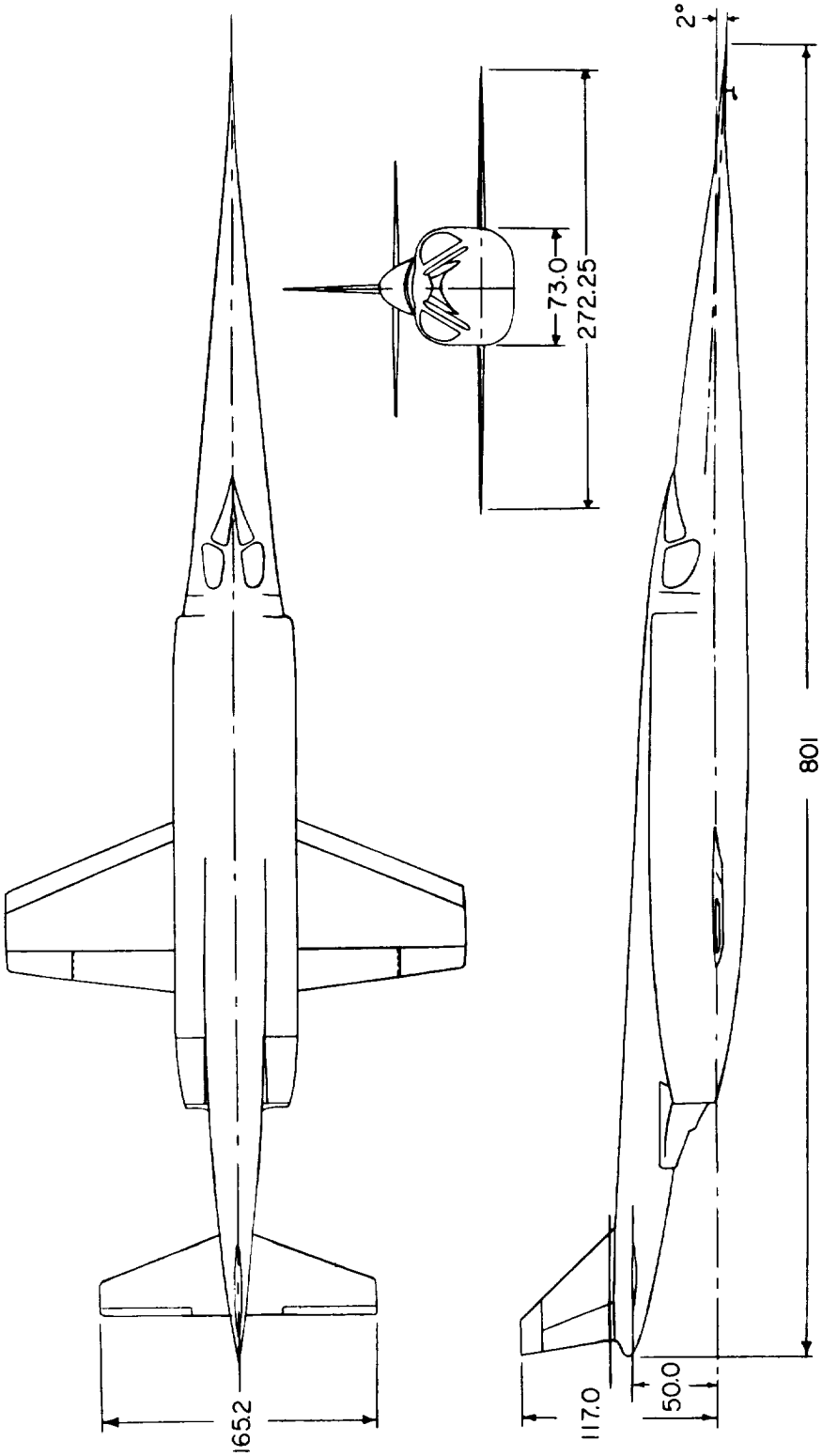

Figure 3.- Three-view drawing of the X-3 airplane. All dimensions in inches.

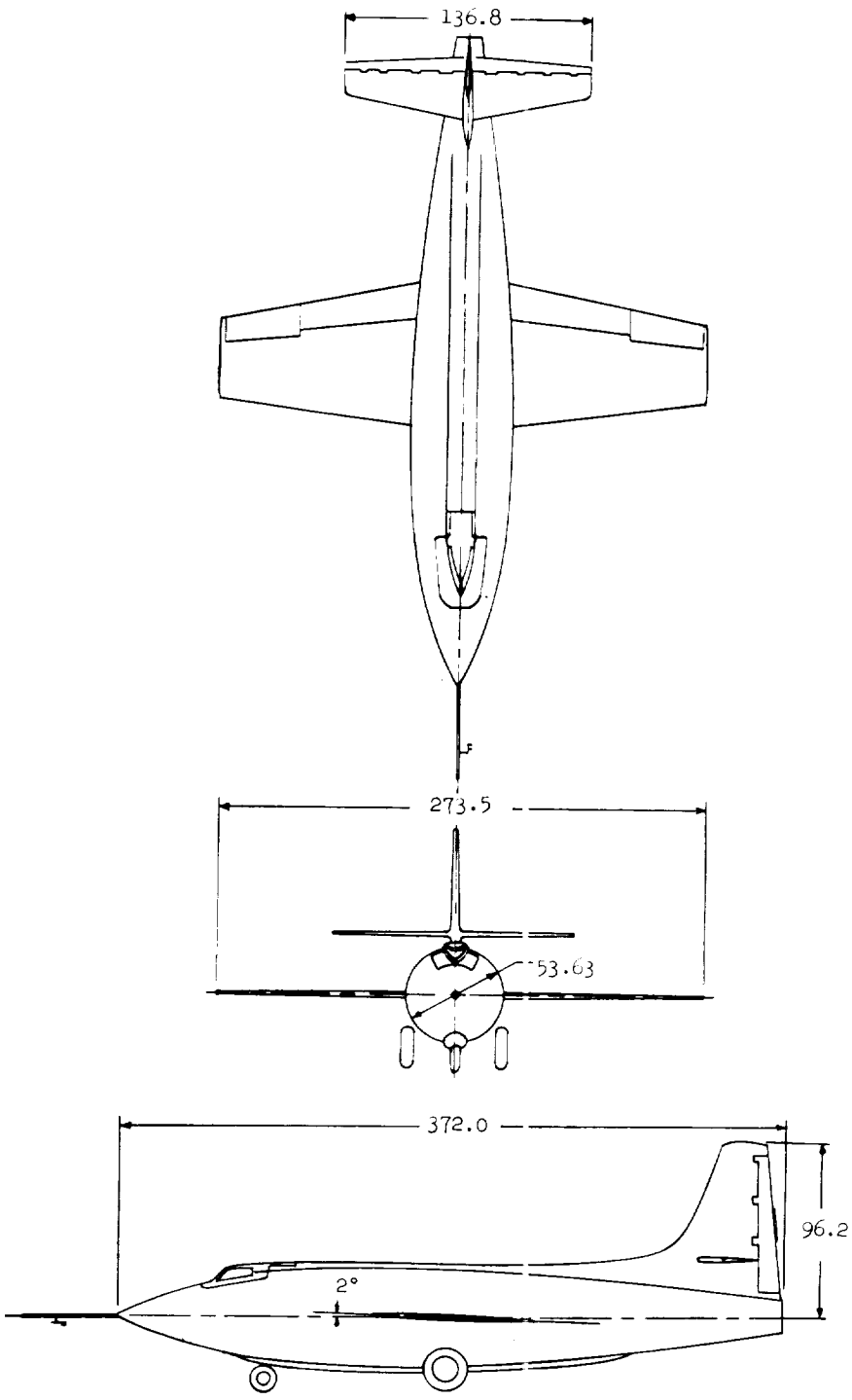

Figure 4.- Three-view drawing of the X-1E airplane. All dimensions in inches.

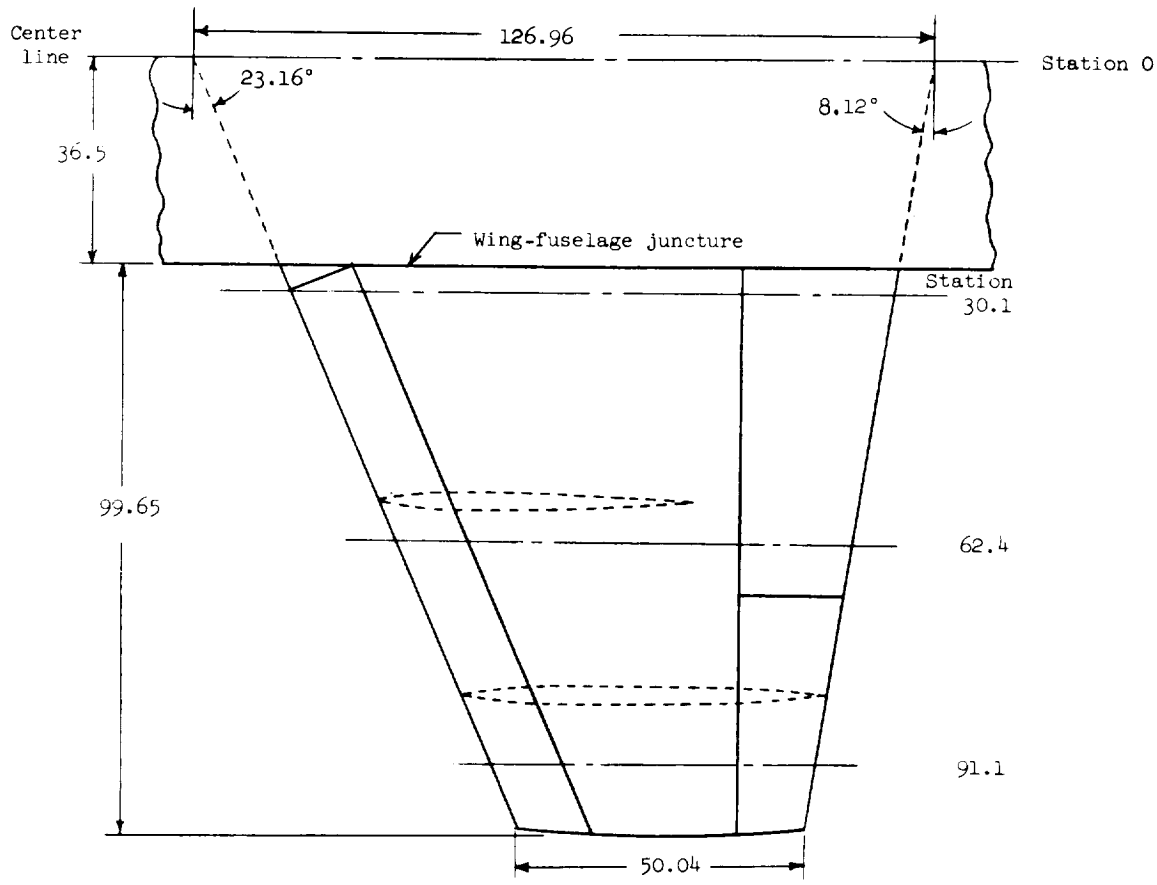

Figure 5.- Left wing of the X-3 airplane showing location of orifice rows.

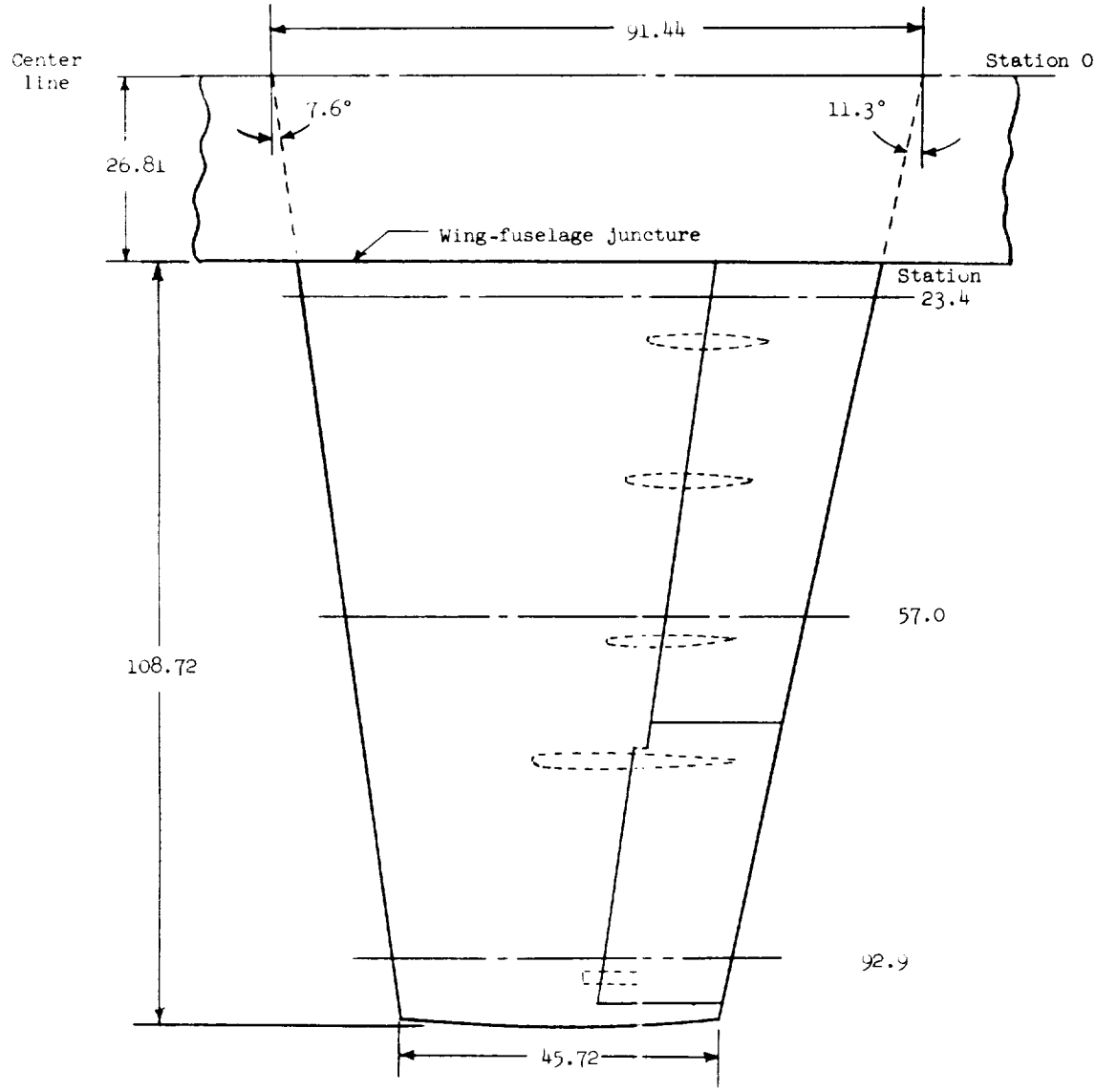

Figure 6.- Left wing of the X-1E airplane showing location of orifice rows.

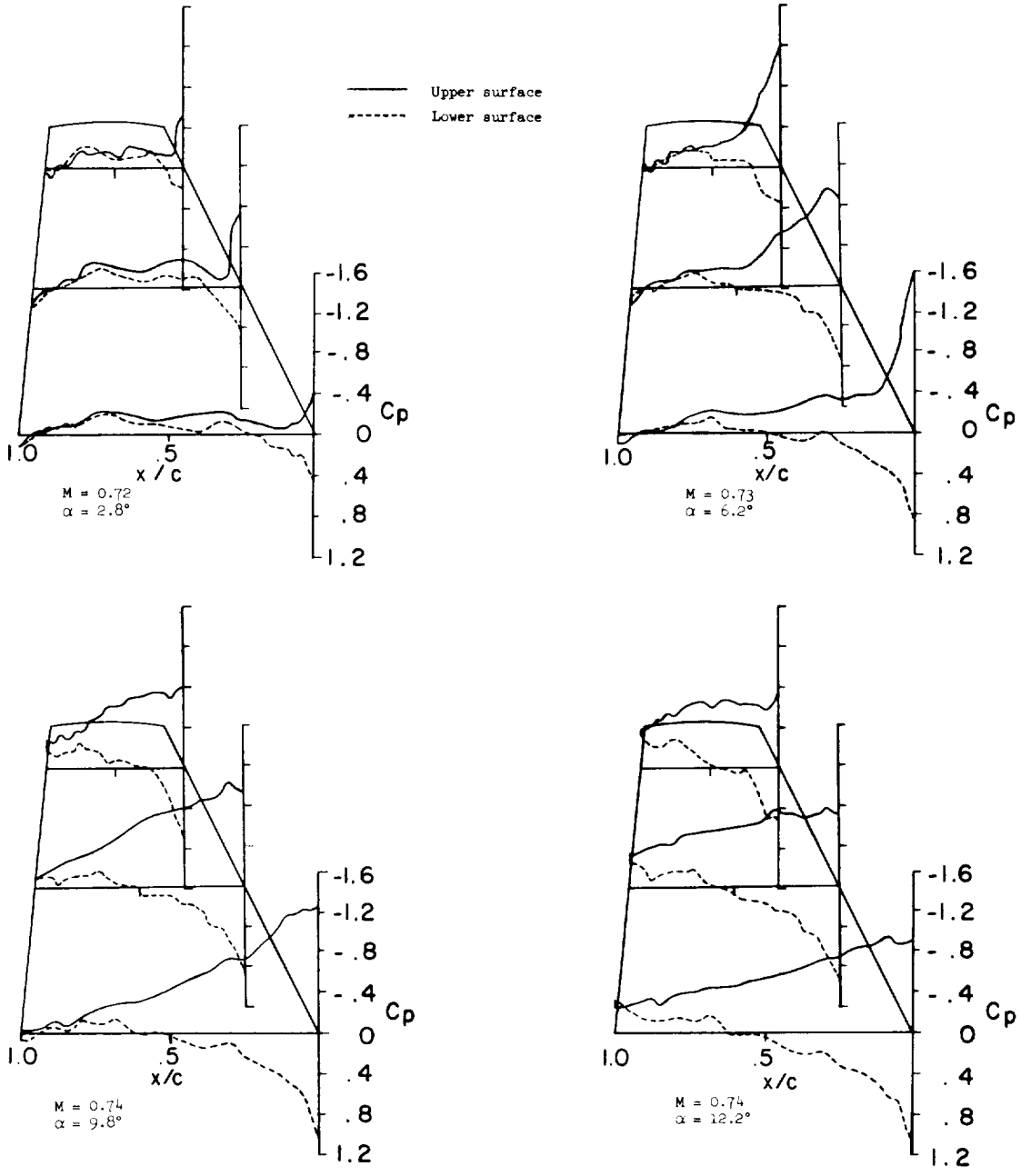

(a) $M \approx 0.73$; $C_{p_{cr}} \approx -0.675$.

Figure 7.- Wing plan views showing the effect of increasing angle of attack on the pressure distribution; X-3.

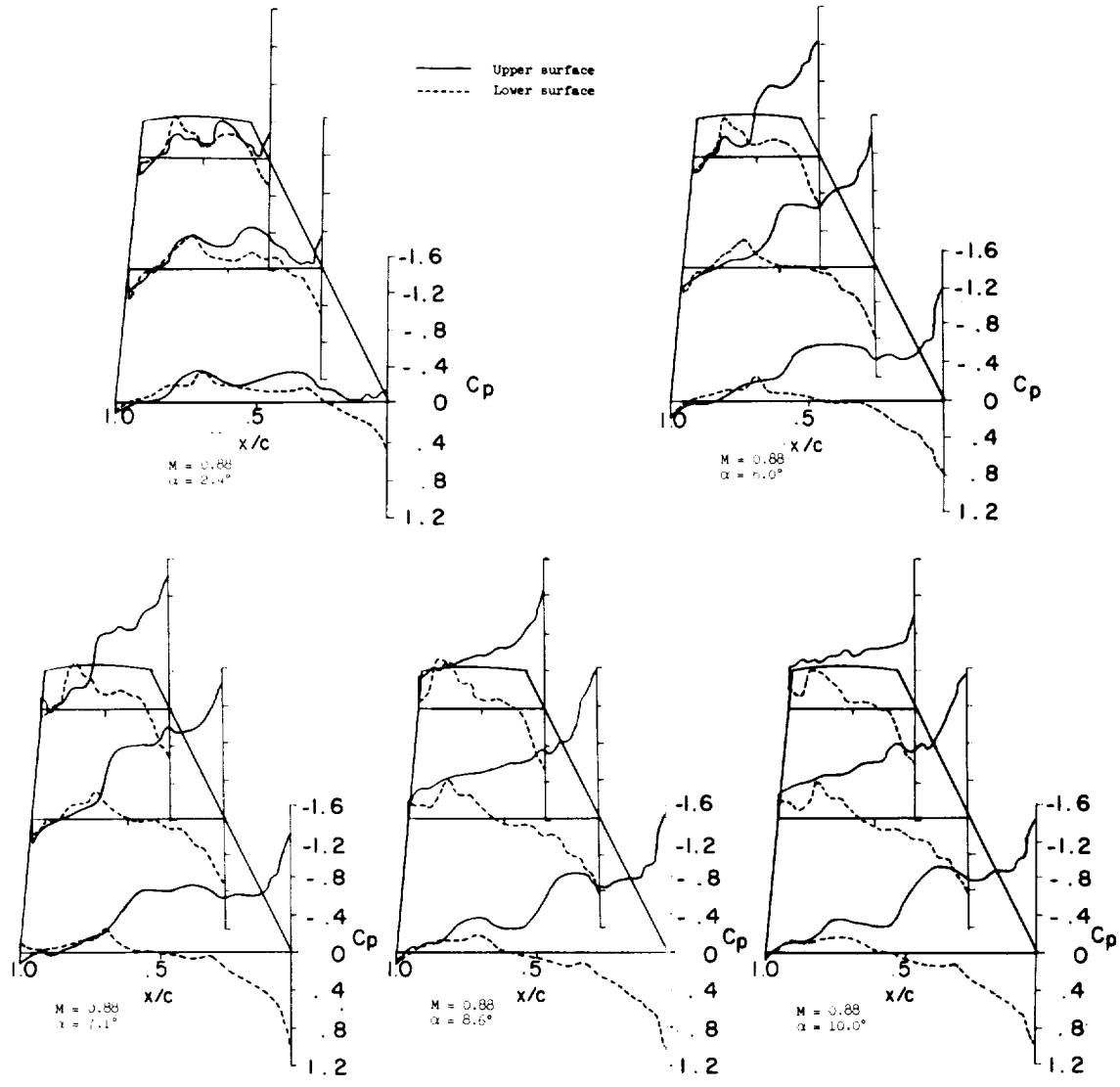

(b) $M \approx 0.88$; $C_{p_{cr}} \approx -0.225$.

Figure 7.- Continued.

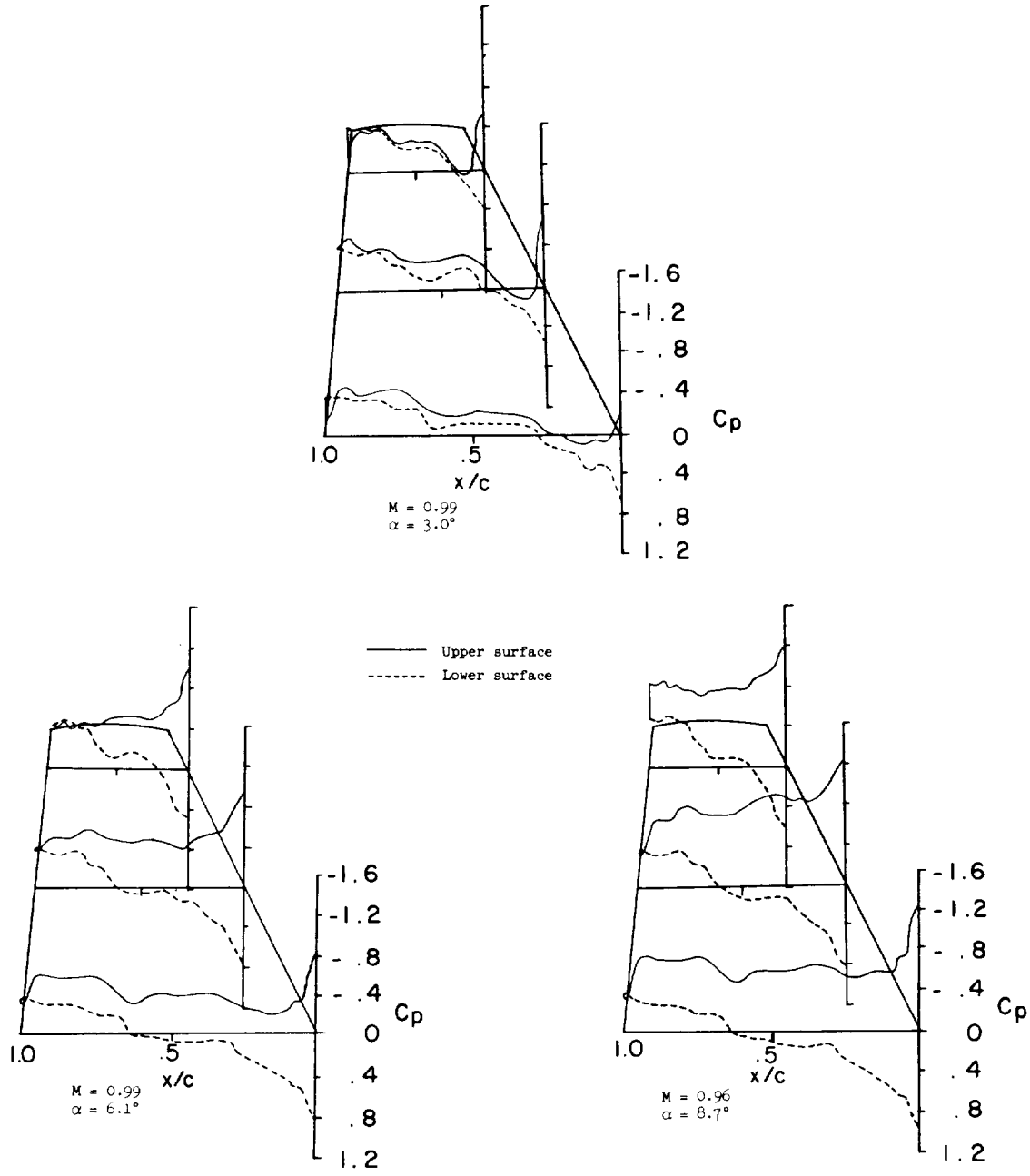

(c) $M \approx 0.99$; $C_{p_{cr}} \approx -0.015$.

Figure 7.- Continued.

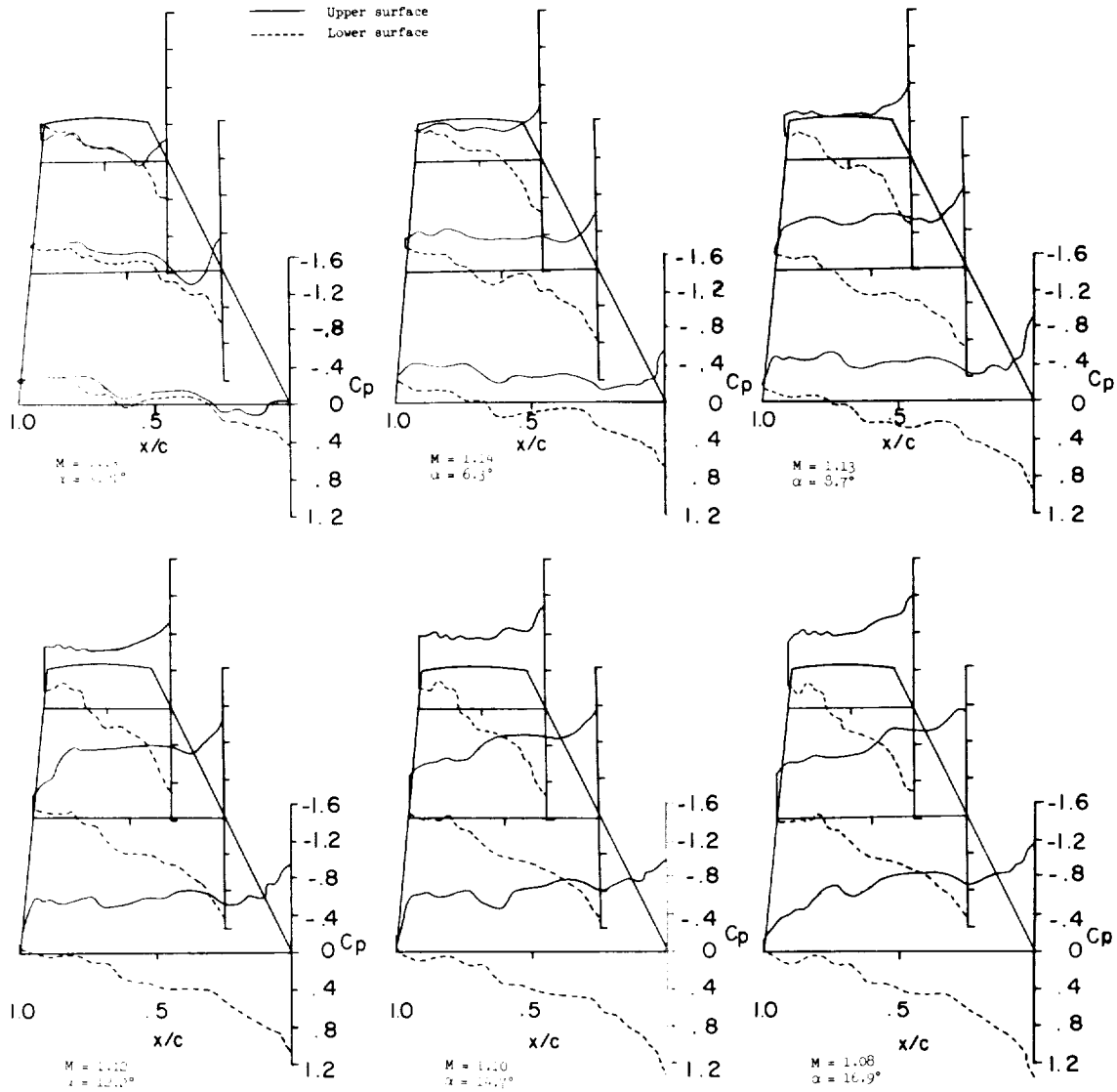

(d) $M \approx 1.13$.

Figure 7.- Concluded.

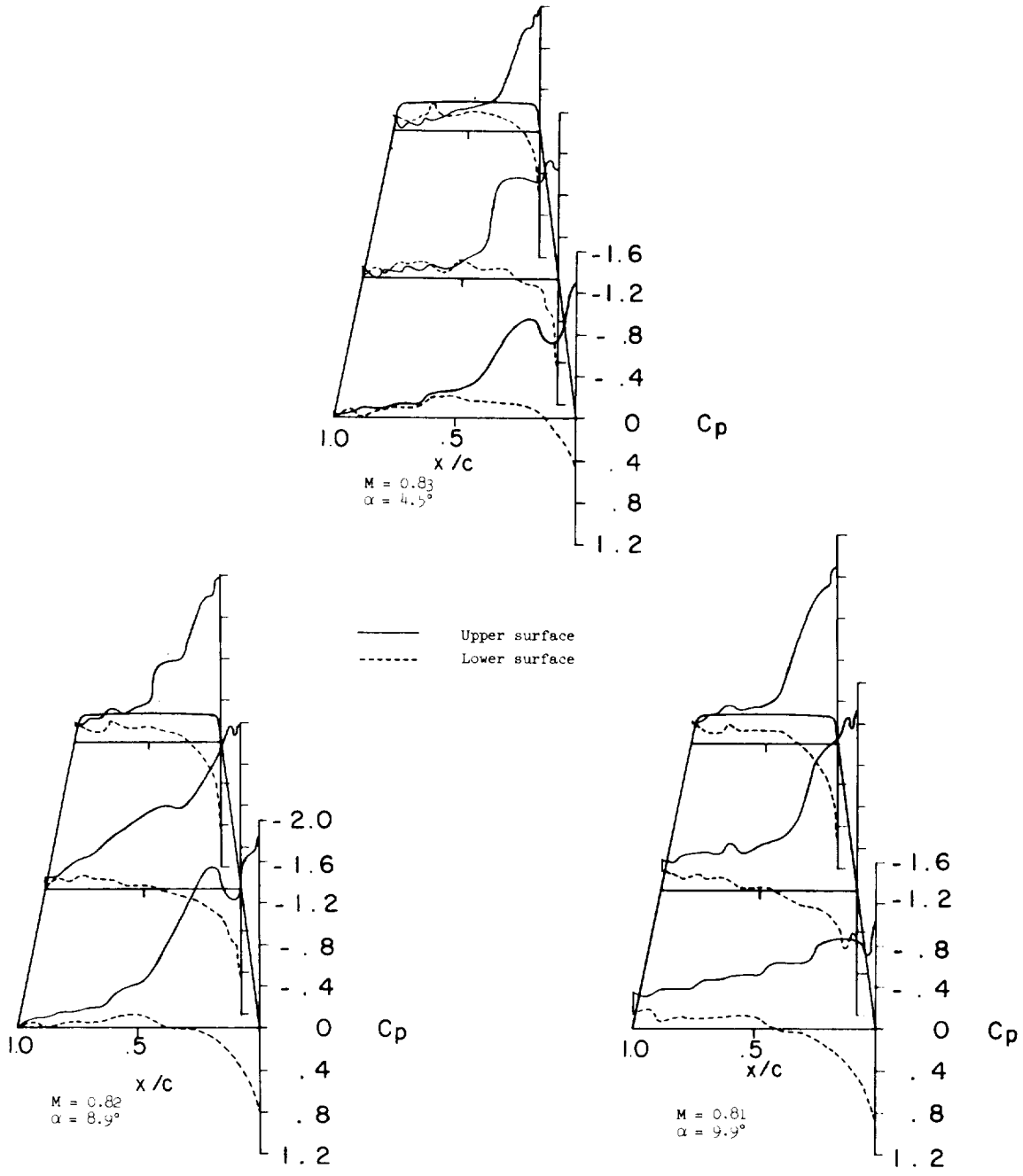

(a) $M \approx 0.82$; $C_{p_{cr}} \approx -0.370$.

Figure 8.- Wing plan view showing the effect of increasing angle of attack on the pressure distribution; X-1E.

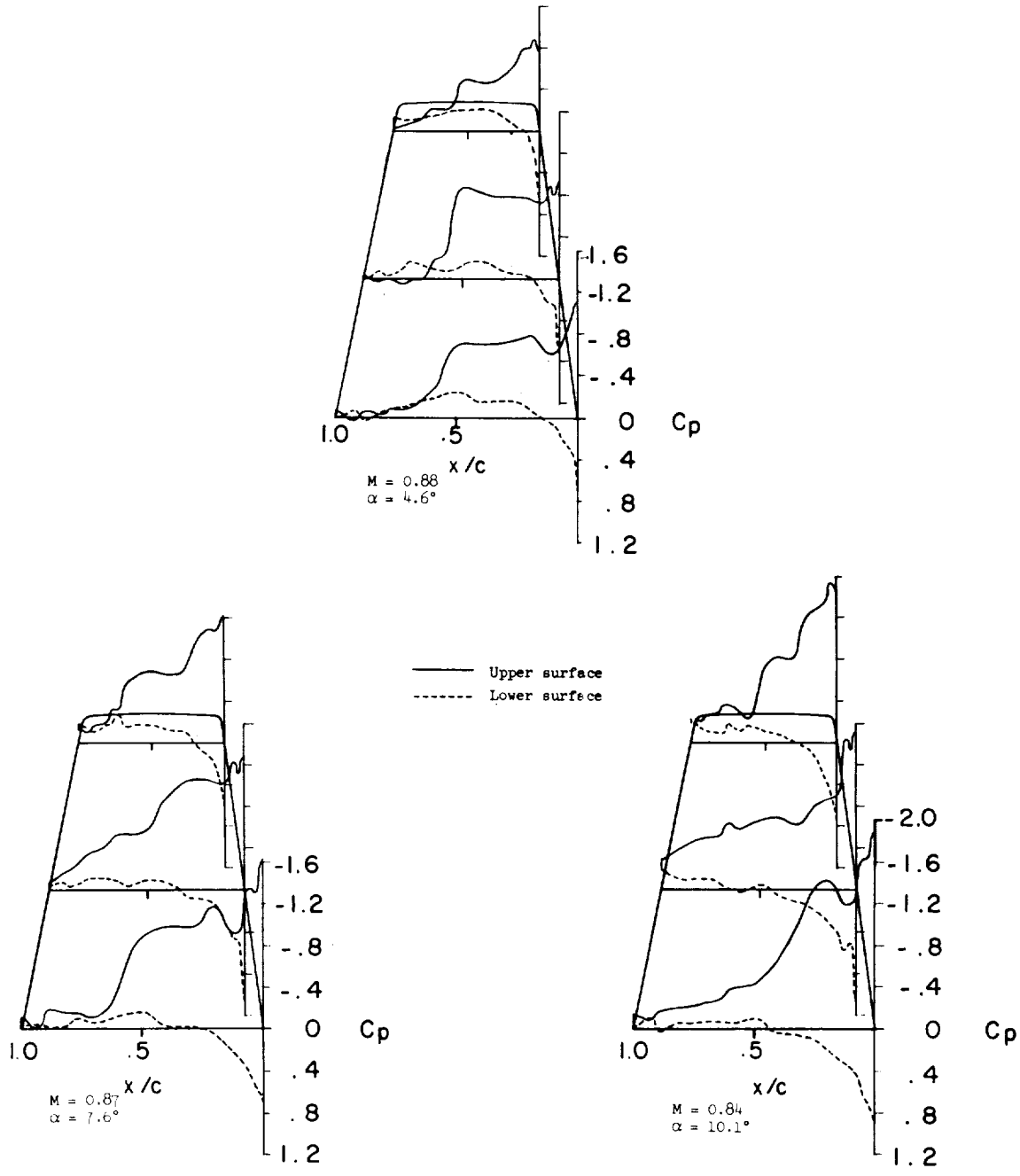

(b) $M \approx 0.88$; $C_{p_{cr}} \approx -0.225$.

Figure 8.- Continued.

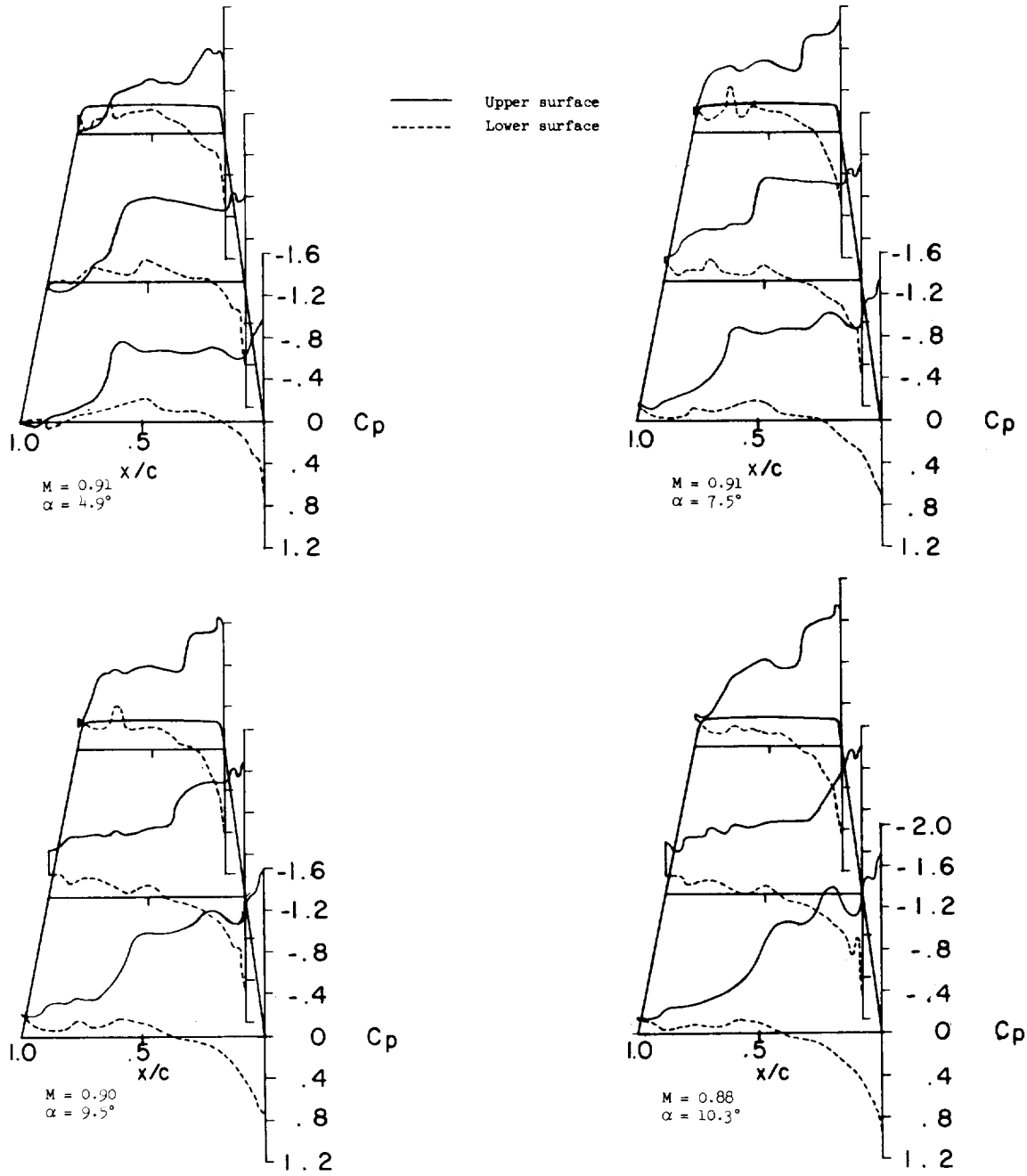

(c) $M \approx 0.90$; $C_{p_{cr}} \approx -0.185$.

Figure 8.- Continued.

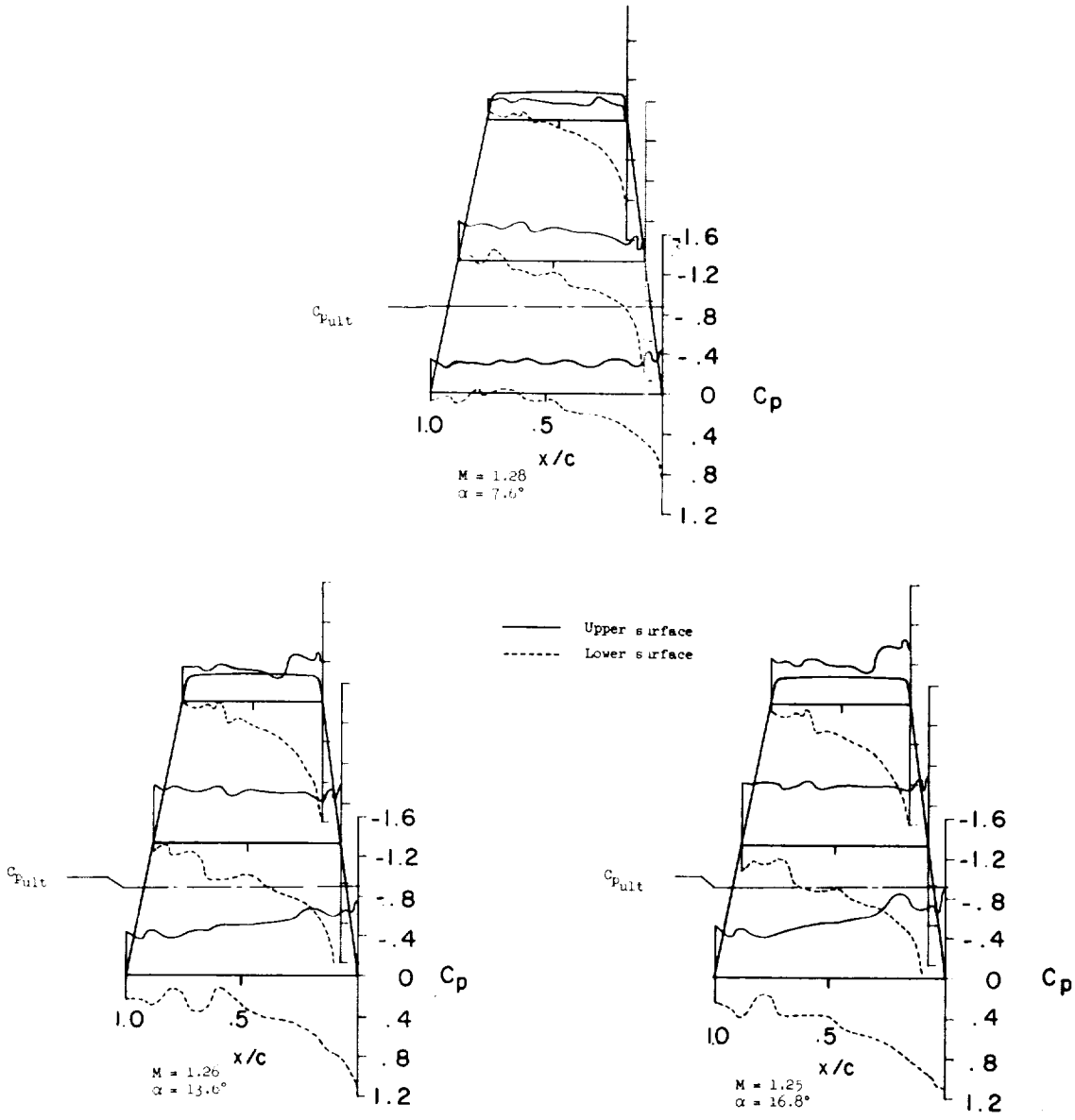

(d) $M \approx 1.25$.

Figure 8.- Continued.

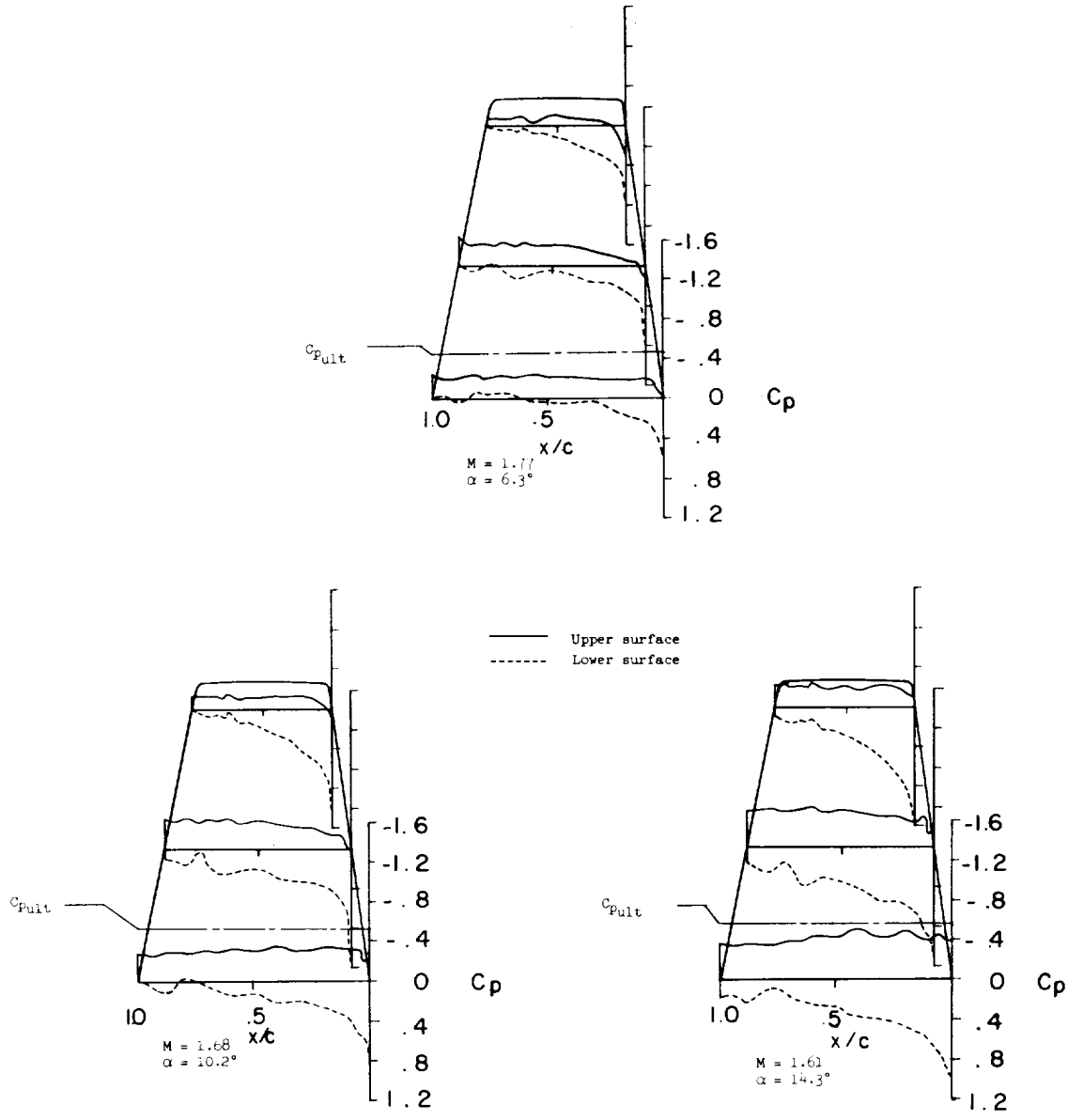

(e) $M \approx 1.70$.

Figure 8.- Continued.

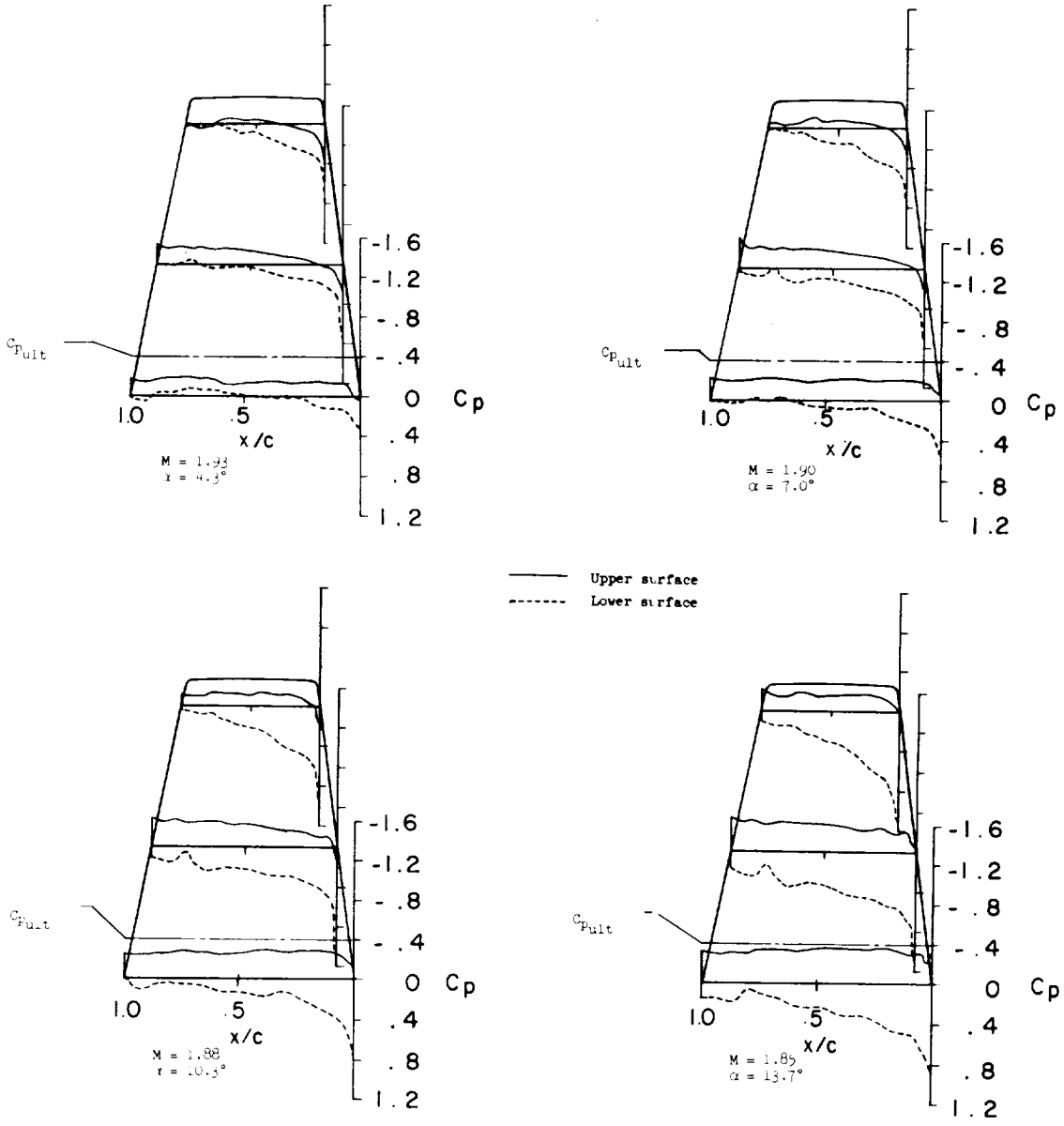

(f) $M \approx 1.90$.

Figure 8.- Concluded.

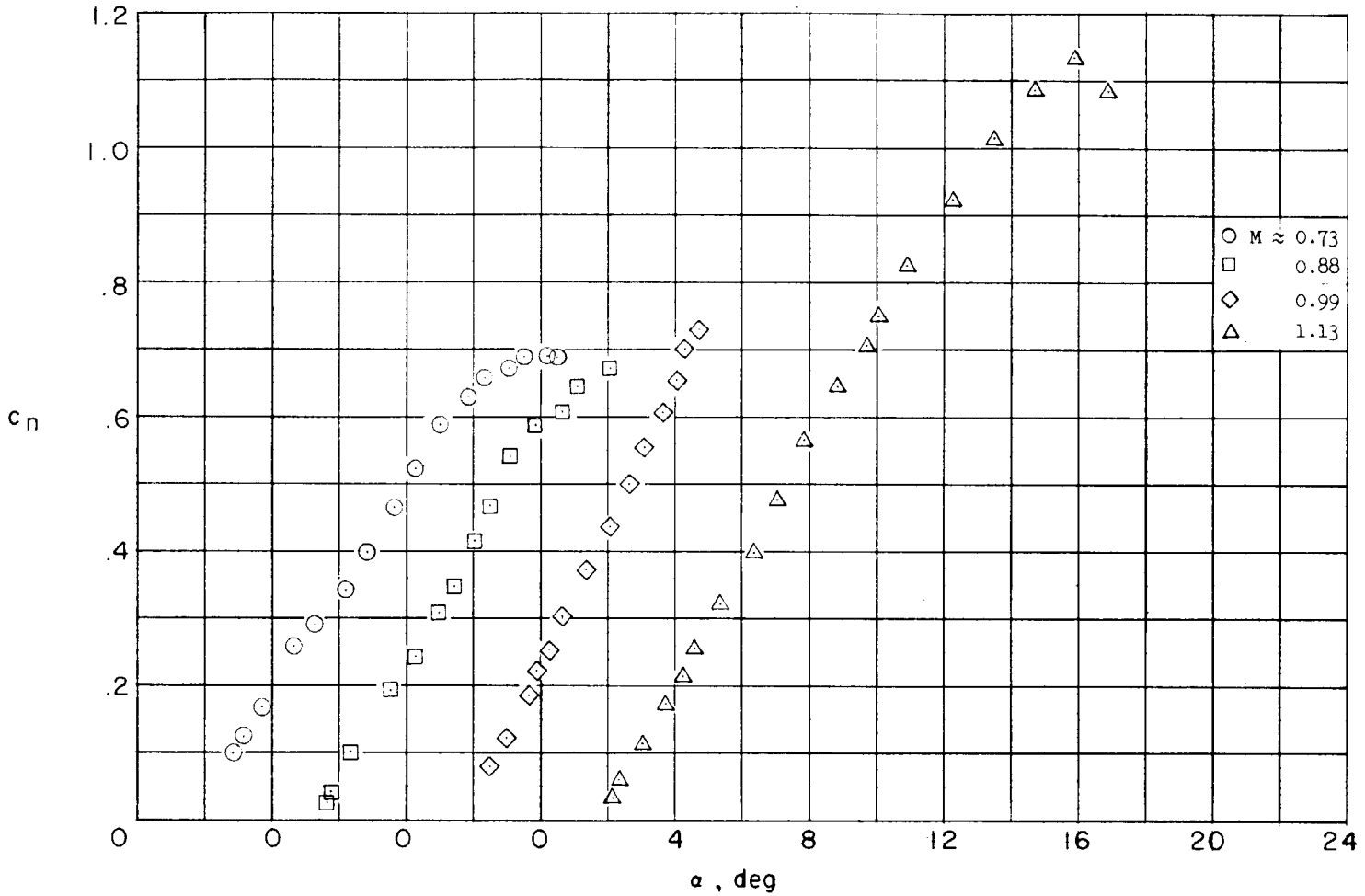

(a) Root station.

Figure 9.- Variation of section normal-force coefficient with airplane angle of attack at several Mach numbers; X-3.

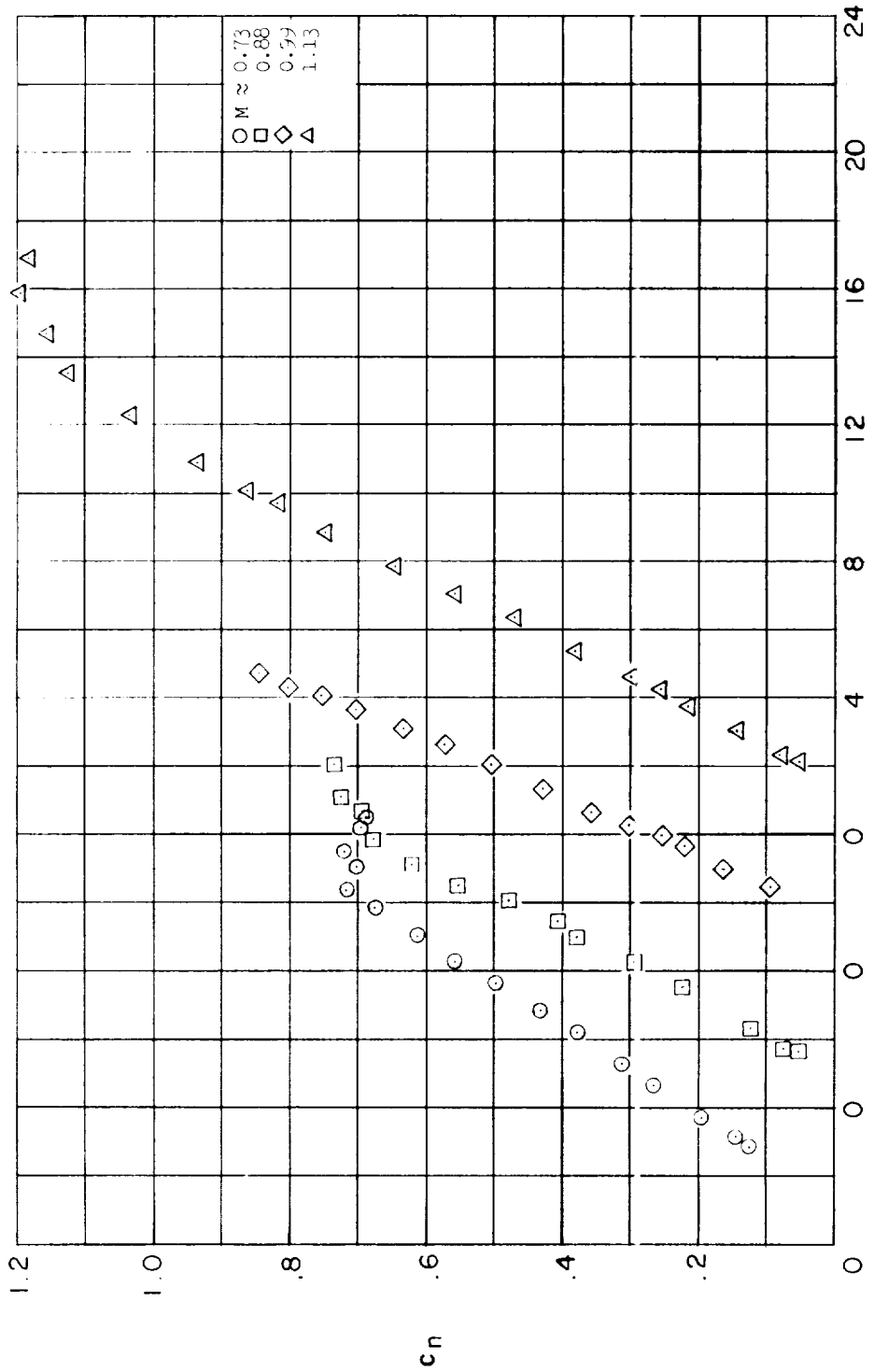

(b) Midsemispan station.

Figure 9.- Continued.

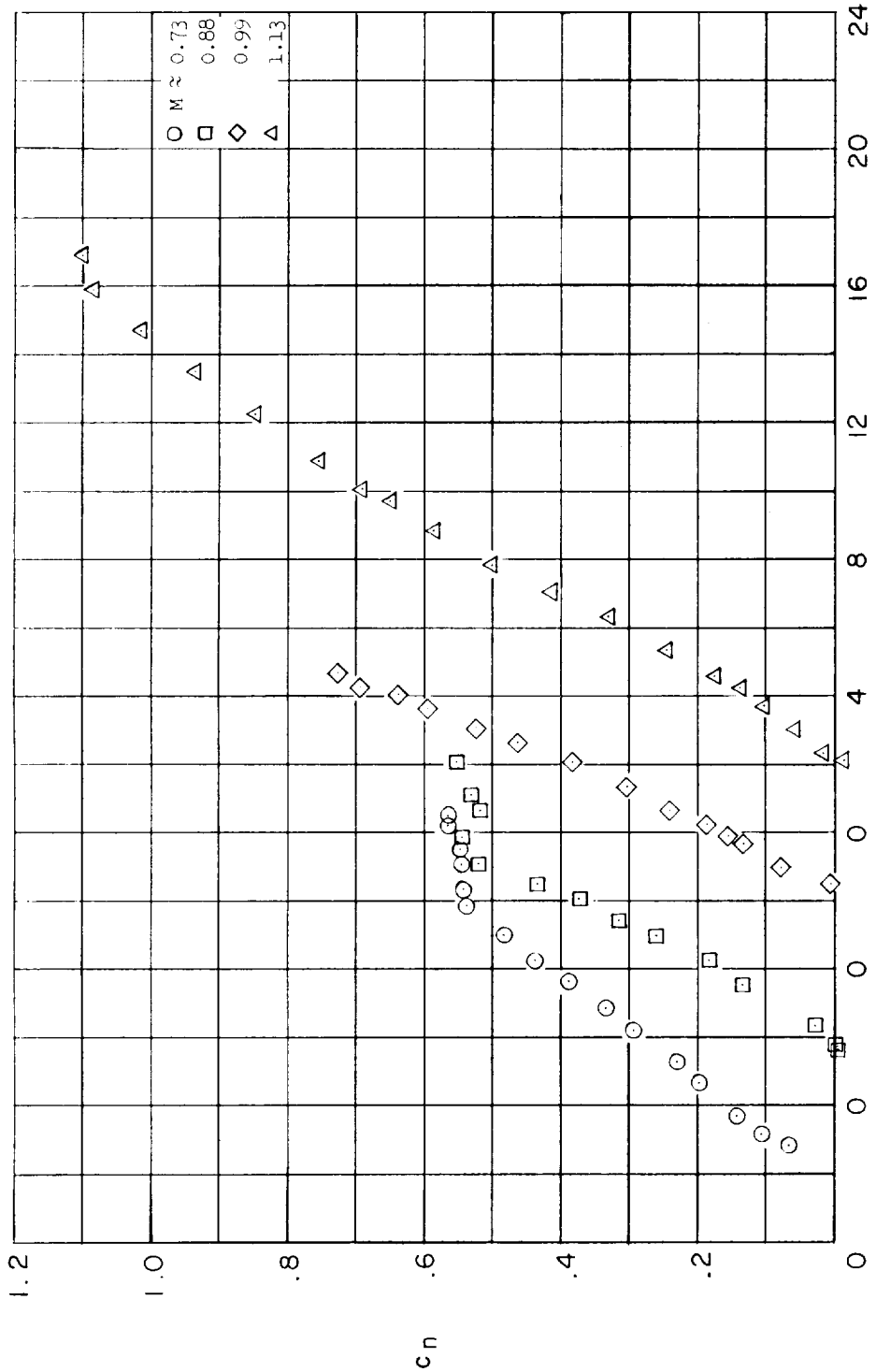

(c) Tip station.

Figure 9.- Concluded.

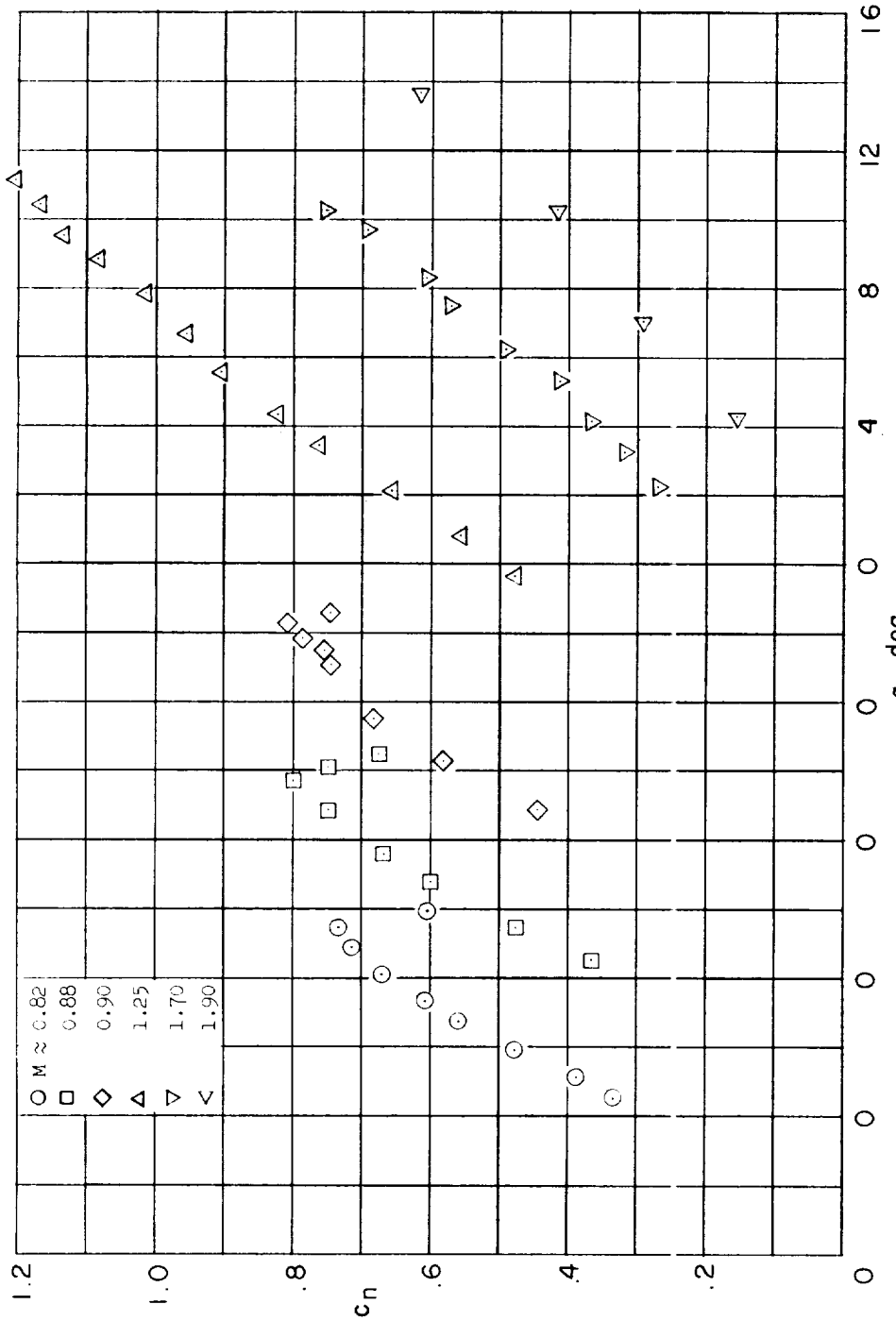

(a) Root station.

Figure 10.- Variation of section normal-force coefficient with airplane angle of attack at several Mach numbers; X-1E.

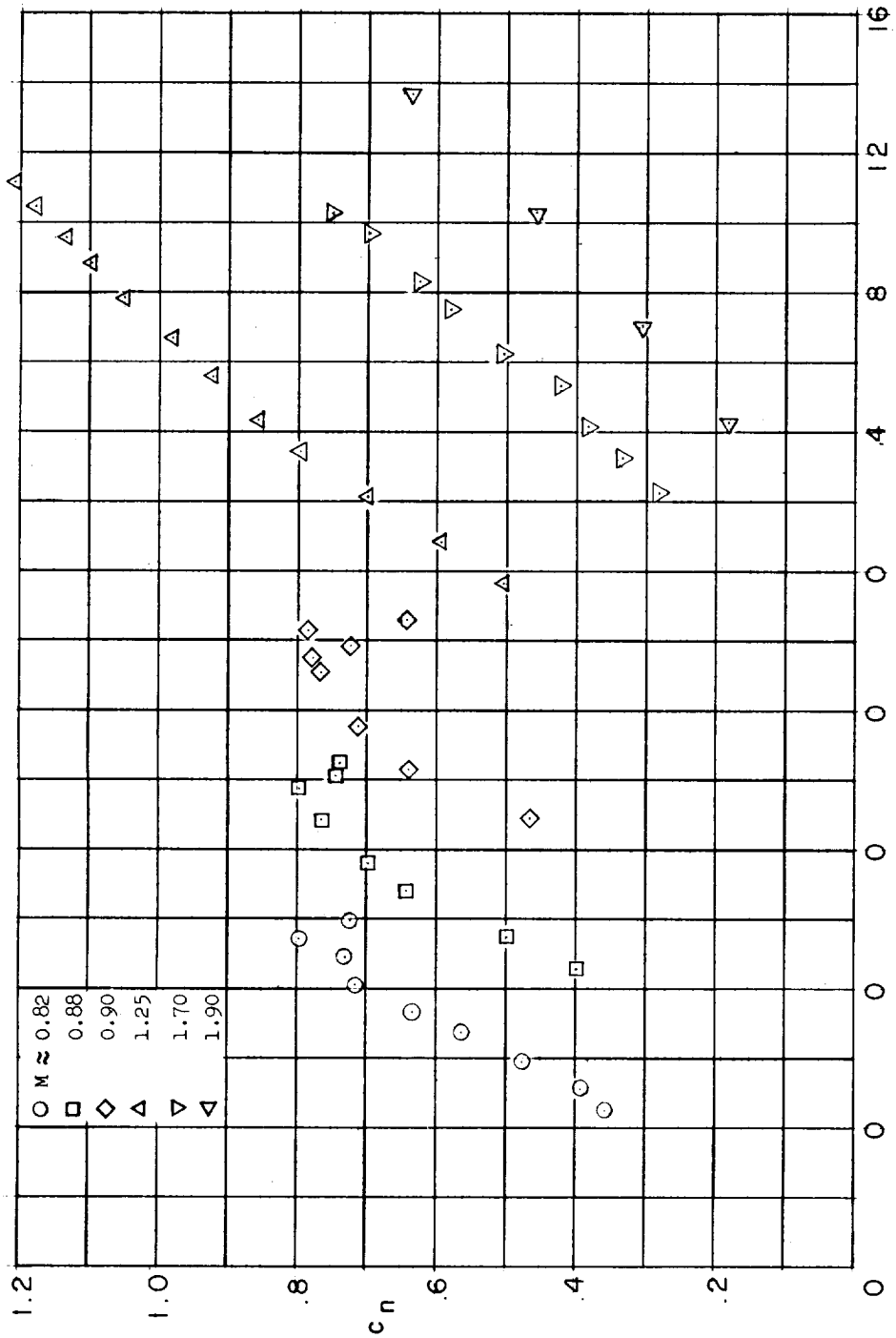

(b) Midsemispan station.

Figure 10.- Continued.

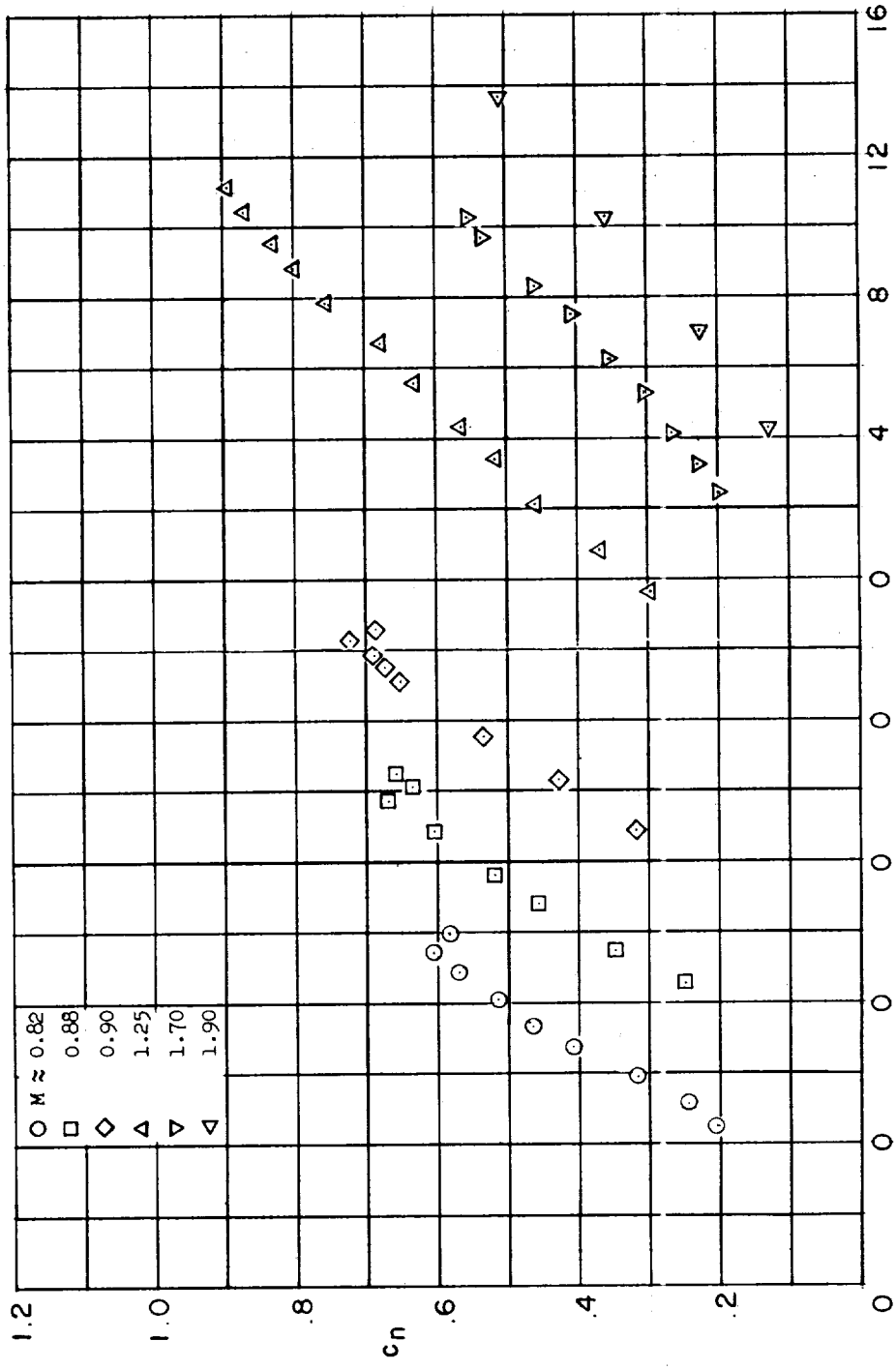

(c) Tip station.

Figure 10.- Concluded.

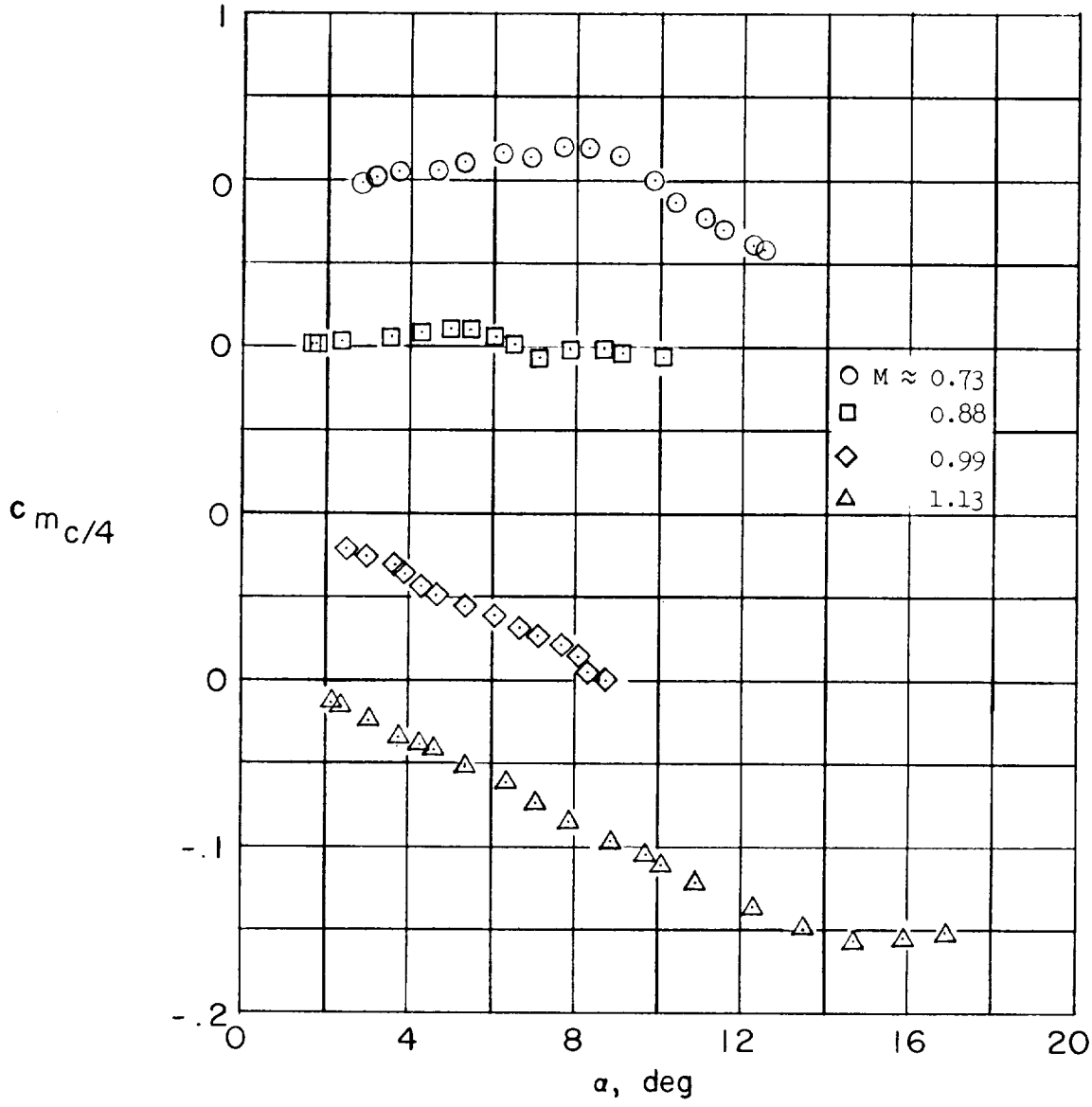

(a) Root station.

Figure 11.- Variation of section pitching-moment coefficient with airplane angle of attack at several Mach numbers; X-3.

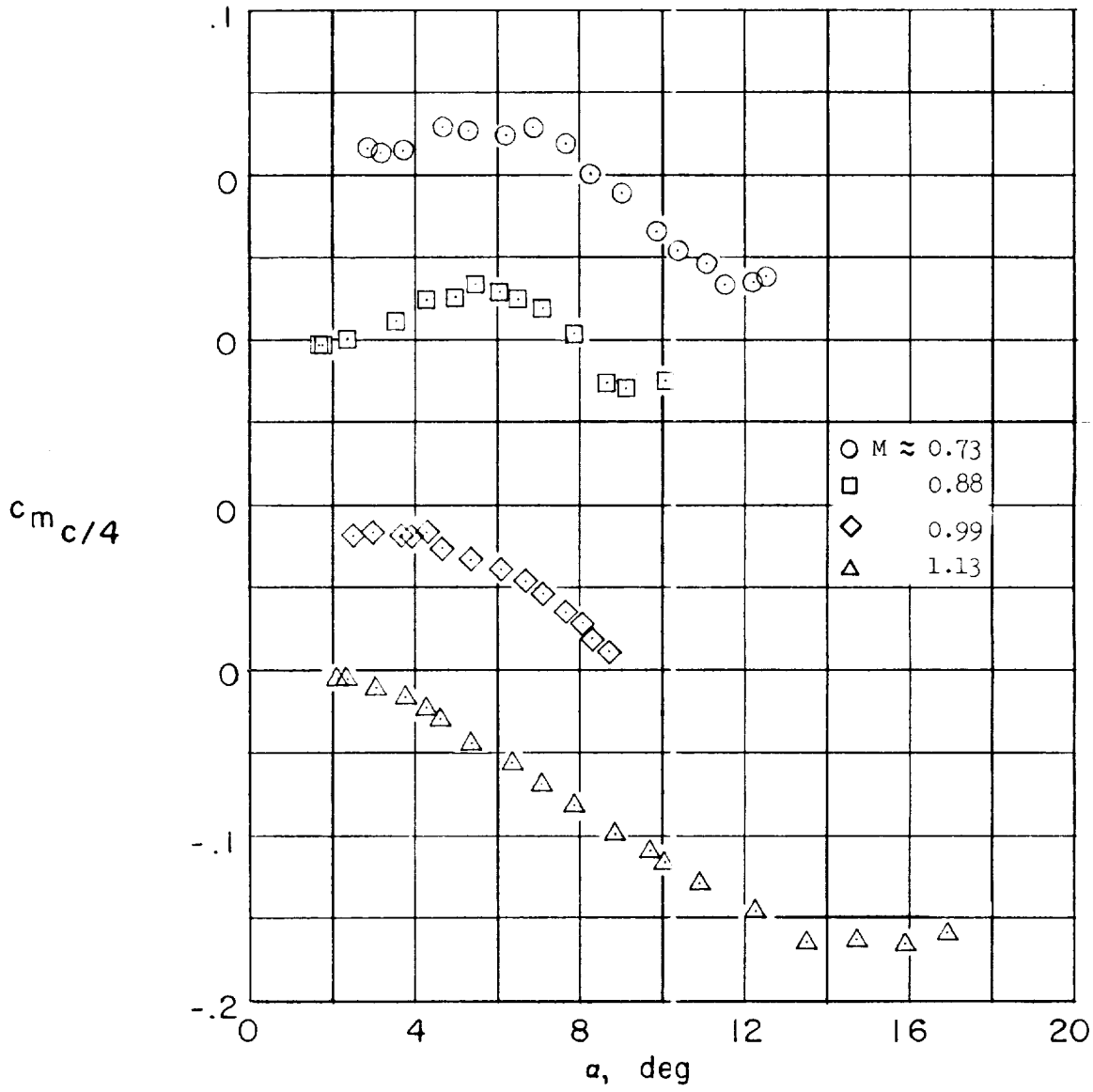

(b) Midsemispan station.

Figure 11.- Continued.

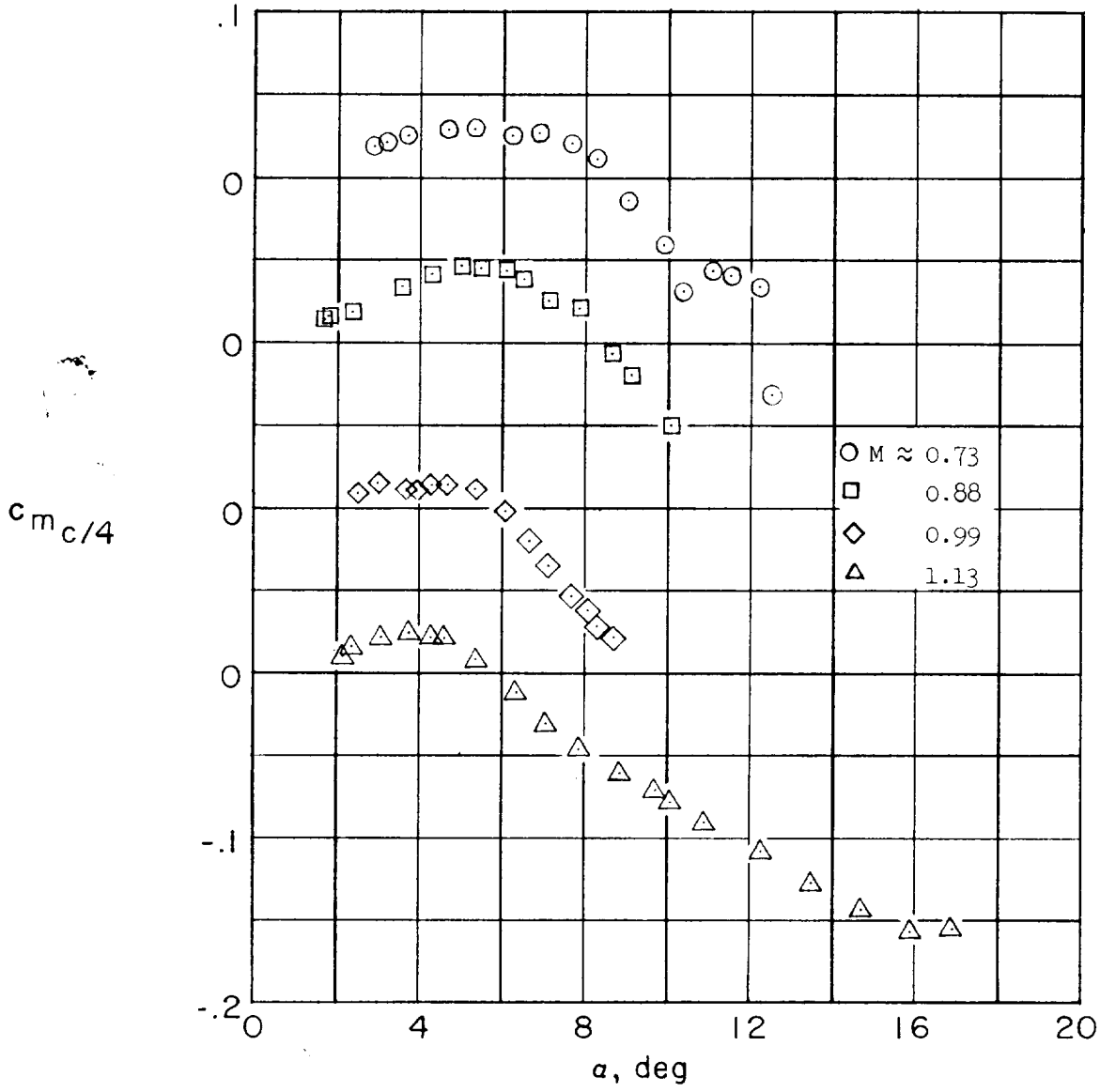

(c) Tip station.

Figure 11.- Concluded.

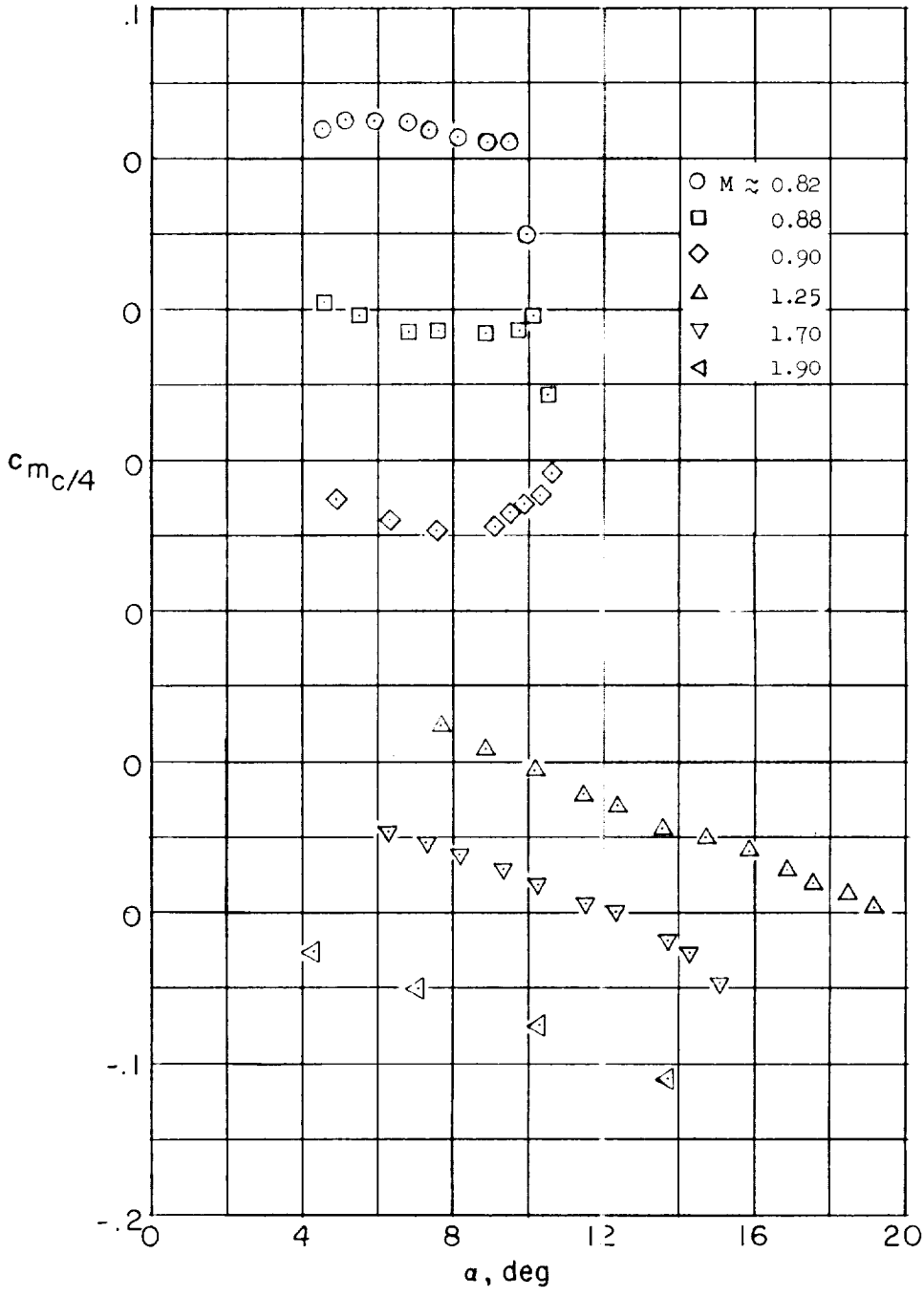

(a) Root station.

Figure 12.- Variation of section pitching-moment coefficient with airplane angle of attack at several Mach numbers; X-1E.

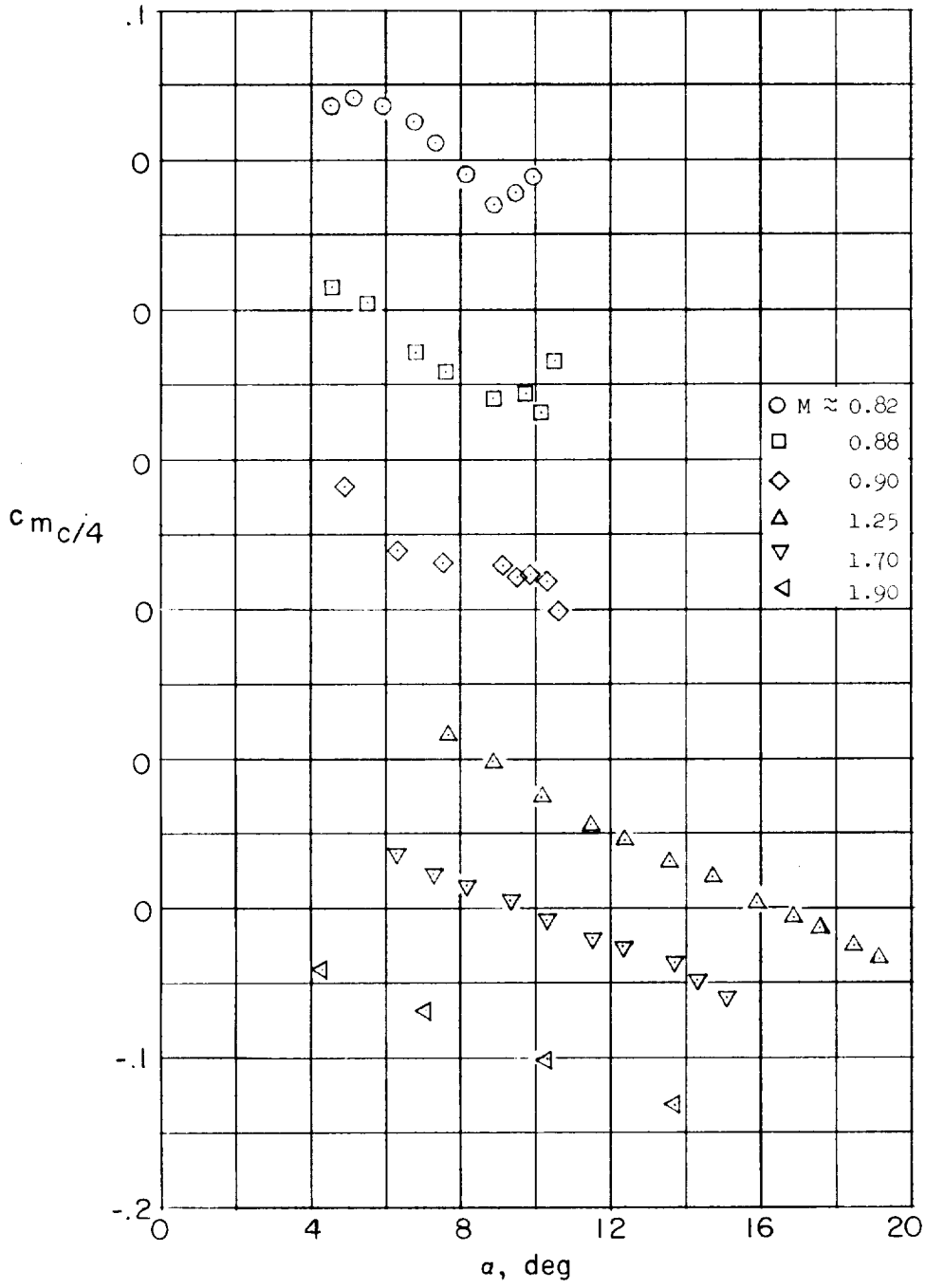

(b) Midsemispan station.

Figure 12.- Continued.

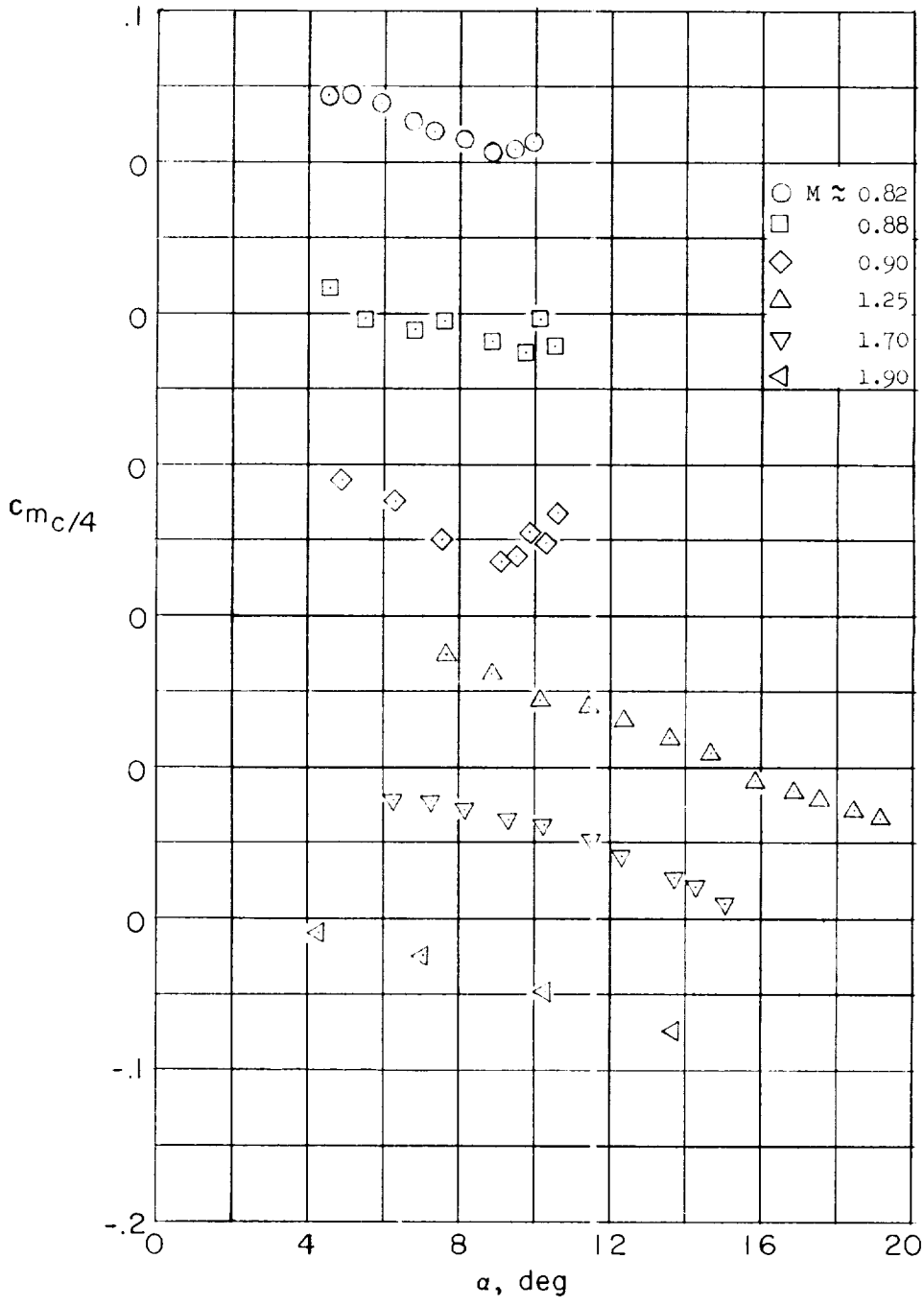

(c) Tip station.

Figure 12.- Concluded.